

Anders Guldal Bramness

# Computational Analysis of a Double-sided Linear Induction Motor for a Hyperloop Transportation System

Master's thesis in Energy and Environmental Engineering

Supervisor: Jonas K. Nøland

June 2023



Anders Guldal Bramness

# **Computational Analysis of a Double-sided Linear Induction Motor for a Hyperloop Transportation System**

Master's thesis in Energy and Environmental Engineering  
Supervisor: Jonas K. Nøland  
June 2023

Norwegian University of Science and Technology  
Faculty of Information Technology and Electrical Engineering  
Department of Electric Power Engineering





# Computational Analysis of a Double-sided Linear Induction Motor for a Hyperloop Transportation System

Anders Guldal Bramness  
 Department of Electric Energy  
 Norwegian University of Science and Technology  
 Trondheim, Norway  
 andergb@stud.ntnu.no  
 Supervisor: Jonas Kristiansen Nøland (NTNU)

**Abstract**—This thesis aimed to explore a mode of propulsion for a Hyperloop Transportation System (HTS) in its critical start-up phase. A big challenge facing the revolutionary transportation system is the cost and weight of the powertrain. The Linear Induction Motor (LIM) is thought to be a good option due to its low implementation cost, though the efficiency is questionable. Breakthroughs in Finite Element Analysis (FEA) allow for detailed simulations of computer-generated models of the powertrain. A two-dimensional (2D) model of the LIM was built for the thesis in order to study the performance at low frequencies corresponding to the motor's acceleration period. Moreover, analytical simulations in Simulink were done based on the theory transferred from conventional induction motors, and transient results were made to further understand the meaning of the stationary results, as well as comprehend the real behavior of the LIM. The results showed that the analytical results generally had the highest thrust force and efficiency, as the LIM in these simulations was simplified. The transient results showed a resemblance to the stationary results, with a significant ripple at the lowest operating speeds, which grew as the speed was increased. It is likely that these were caused by step responses from zero initial conditions. Further work needs to be done by reducing the ripple through a better design and analysis over longer computation times.

## NOMENCLATURE

### Abbreviations

DLIM	Double-sided Linear Induction Motor
FEA	Finite Element Analysis
HTS	Hyperloop Transportation System
IM	Induction Motor
LIM	Linear Induction Motor
Maglev	Magnetic Levitation
RIM	Rotary Induction Motor
SLIM	Single-sided Linear Induction Motor

### Electrical parameters

$\cos(\phi)$	Power factor
$\eta$	Efficiency
$\sigma_{Al}$	Conductivity of aluminium
$\sigma_{Cu}$	Conductivity of copper
$f$	Electrical frequency
$I$	Current
$i_1(t)$	Primary current - instantaneous

$I_1$	Primary current - RMS
$I_2'$	Secondary current referred from the primary
$I_{DC}$	DC Current
$I_{max}$	Maximum current
$J_0$	Current density
$k, a, c$	Constants for Steinmetz' equation
$k_N$	Primary winding factor
$m$	Number of phases
$N$	Number of primary windings
$P$	Power
$P_{ag}$	Air gap power
$P_{cu}$	Conduction/Copper losses
$P_{in}$	Input power
$P_{loss}$	Arbitrary loss type of the machine
$P_{mech}$	Mechanical power
$P_{total}$	Total power losses in the machine
$R$	Resistance
$R_1$	Primary resistance
$R_2'$	Secondary resistance referred from the primary
$R_{cu}$	Copper resistance
$R_C$	Core resistance
$R_{measured}$	Measured resistance at a no-load/locked rotor test
$S$	Supplied apparent power
$u_1(t)$	Primary voltage - instantaneous
$U_1$	Primary voltage - RMS
$U_{DC}$	DC Voltage
$X_1$	Primary reactance
$X_2'$	Secondary reactance referred from the primary
$X_m$	Magnetizing reactance
$X_{measured}$	Measured reactance at a no-load/locked rotor test
<b>Geometry</b>	
$2a$	Stator width/Model depth
$\tau_p$	Pole pitch
$FF$	Fill factor
$g$	Air gap
$h_{air}$	Air domain margin height
$h_{Al}$	Thickness of secondary aluminum rail
$L_{Al}$	Length of secondary aluminum rail
$w_s$	Slot width

$w_t$  Tooth width  
 $w_{air}$  Air domain margin width

**Mechanical parameters**

$F$  Thrust force  
 $n_s$  Rotational synchronous speed  
 $s$  Slip  
 $v$  Speed of the motor  
 $v_s$  Synchronous speed

I. INTRODUCTION

The Hyperloop Transportation System (HTS) has been an exciting prospect since its relaunch by Elon Musk in 2011 as a future means of transportation [1]. By having a capsule levitate and travel along a partially evacuated tube, the mechanical resistance forces of drag and friction can be reduced or even removed entirely, reaching speeds on land up to 1200 km/h [2]. However, for the HTS to be realized, its cost of implementation and maintenance must be lowered significantly [3]. While some companies have planned and developed prototypes with existing technology [4], more research is still needed. In particular, one of the few technologies thought to be economically feasible is the use of Linear Induction Motors (LIM) [5]. They are cheap to produce compared to other technologies and have a low electrification cost [6], as well as good synergy with the inherently stable Electrodynamic Suspension [7]. Unfortunately, the efficiency and thrust force is among the lowest of HTS propulsion technologies [8], making the operating cost high. That being said, potential breakthroughs are still possible to analyze.

So far, LIM has been studied for use in traditional as well as Magnetic Levitation (Maglev) transportation [9]- [11]. The theory regarding LIM side effects has been studied with regards to transportation [12]- [14], and stationary simulations have been done with programs using Finite Element Analysis (FEA) of both 2D and 3D Models [15]- [18].

This thesis aimed to further explore the acceleration of a LIM at low frequencies, as this is where the demands for propulsion are the highest and is therefore a bottleneck. The theory and characteristics of LIM were explained to establish a basis for analytical results. A 2D model was created in a FEA program (COMSOL), and stationary as well as time-dependent studies were performed. Study parameters of interest were when the motor was at its maximum efficiency and/or thrust force. The analytical, stationary, and time-dependent results were compared to understand the connection between stationary and time-dependent simulations. This way, the goal was to clarify if LIM is feasible for HTS.

II. THEORETICAL BACKGROUND

A. The Linear Induction Motor – a brief summary

While the relaunch of HTS as a potential mode of transportation has inspired new research for only a little more than a decade, the LIM is in comparison well researched. The concept of a LIM is similar to a standard Induction Motor (IM), also known as a Rotary Induction Motor (RIM) to underline the difference, with the obvious difference of producing a linear

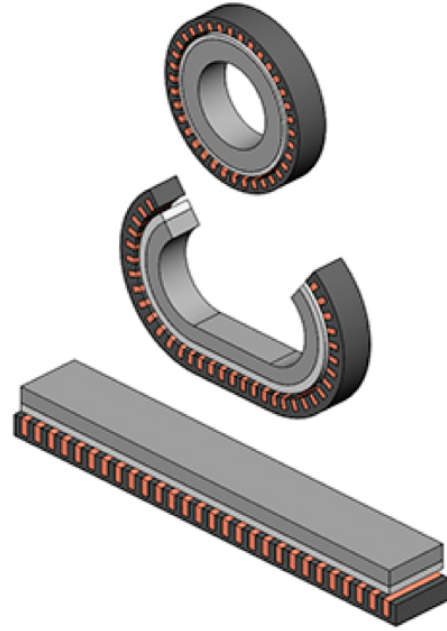


FIGURE 1: The relation of a conventional motor and a LIM. The motor is cut open and rolled out flat to convert rotary to linear motion. [19].

instead of a rotary motion. This is done by having the stator of a RIM cut open and rolled out to a flat shape, as seen in Figure 1.

Since the LIM produces a linear motion, the motor’s “rotor” is a metal beam or sheet instead of a cylindrical ferromagnetic core. Note that the terminology when describing a LIM is slightly different than a RIM. As the mechanical motion is no longer rotary, the wired half of the motor is called the *primary*, and the other half of solid metal is called the *secondary*. The relation between the primary and the secondary can be seen in Figure 2. The current flowing through the wires in the primary will now produce a traveling magnetic field instead of a rotary one, inducing currents in the secondary, creating a traveling magnetic field of its own. This will produce some type of mechanical motion, which can happen in either the primary or secondary, allowing for two possible configurations of a LIM [7]. Aside from rotary physical concepts being converted to linear, the physics remains the same. This allows for the theoretical background of a RIM to be transferred to a LIM without much effort.

B. The LIM in the Hyperloop Transportation system

For HTS, it has been established that using a Double-sided Linear Induction Motor (DLIM) is a better option than using a Single-sided Linear Induction Motor (SLIM), for several reasons. Assuming Maglev keeps the pod afloat above the aluminum beam, having a SLIM mounted directly below the pod will create a conflict between levitation and propulsion. For stability purposes, the pod should levitate at a sufficient distance from the beam. However, this large air gap will inevitably reduce the efficiency of the motor. This will increase the energy demands to unsustainable levels. As such, mounting

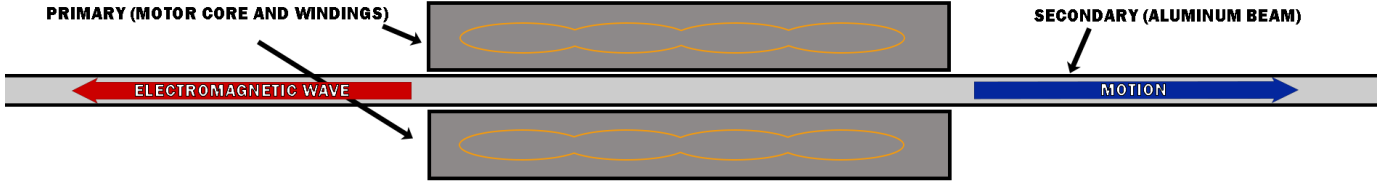


**FIGURE 2:** Bird's eye view of a typical setup of the DLIM primary mounted on an aluminum secondary. The electromagnetic wave and the motion are opposite of each other.

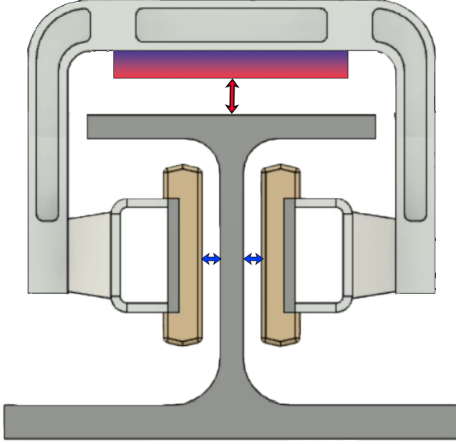


**FIGURE 3:** Cross-section view of a potential setup of a DLIM surrounding an aluminum beam, highlighting the differences between levitation and propulsion air gaps. The levitation air gap is shown with a red arrow, and the propulsion air gaps are shown with blue arrows.

a DLIM on the sides of the aluminum rail will separate the air gaps, and essentially disconnect the levitation from the propulsion, as demonstrated in Figure 3. Note that the systems could also be separated into different rails, i.e. having one set of rails for levitation and one rail for propulsion, if the induced effects of levitation vs. propulsion interferes with each other too much on a single beam.

A DLIM also has practical benefits. For SLIM to be functional for HTS, a ferromagnetic core would need to be installed on the secondary to direct the magnetic field towards it. Whilst for DLIM, the magnetic fields simply pass through the rail between the motors [12]. Having a core mounted on the rail also creates an undesired attraction force between the primary and secondary of the motor, whereas a DLIM does not have that problem [20]. All these advantages make DLIM a valid option as propulsion for HTS.

As mentioned in Section II-A, the theoretical background in RIMs and LIMs are largely the same. However, some differences impact the LIM performance. In addition to the large air gap, shown with blue arrows in Figure 3, the LIM experiences edge effects that are considered parasitic [7]. To understand this, consider that most LIMs have different lengths of the primary and secondary to ensure a continuous operation.

As an example, the aluminum beam a LIM for HTS uses as a secondary is as long as the guideway itself, while the LIM primary is no longer than the length of the pod, as shown in Figure 2. To keep propulsing, currents must be continuously induced in the aluminum beam segment aligning with the primary. As a result, at any given time, new segments with no induced currents are inserted into the motor. Simultaneously, segments already induced create magnetic fields for a short time after the motor has moved past them. The effects of these two phenomena on the motor's performance are respectively called entry effect and end effect, collectively known as edge effects. How substantial these effects are is difficult to determine, with some studies adding constants to account for them when designing a motor [12]. In general, it can be said that they increase with increasing speed of the motor, due to the nature of the effects. As this thesis aimed to explore parameters at low frequencies and thus low speeds, they were not expected to be considerably prevalent.

### C. Analytical theory

Before applying theory from RIMs in LIMs, theoretical differences need to be clarified. For a RIM, the currents produce a rotating magnetic field that has a rotary synchronous speed  $n_s$ , which can be calculated using (1)

$$n_s = \frac{120f}{p} \quad (1)$$

where  $f$  is the electrical source frequency and  $p$  is the number of poles in the motor. As mentioned in Section II-A, the copper windings in a LIM produce a *traveling magnetic field*. By adjusting (1) for linear motion, the linear synchronous speed of the magnetic field,  $v_s$ , can be calculated using (2)

$$v_s = 2 \cdot \tau_p \cdot f \quad (2)$$

where  $\tau_p$  is the pole pitch of the motor.

The induced currents in the secondary will create a traveling magnetic field of its own that will try to catch up with the traveling magnetic field produced by the copper windings. It does this by creating a Lorentz force on the secondary that propels it in the same direction. For a stationary secondary, like an aluminum beam fixed in place, the traveling magnetic field is propelled backward, making the primary thrust forward due to Newton's third law. This is shown in Figure 2.

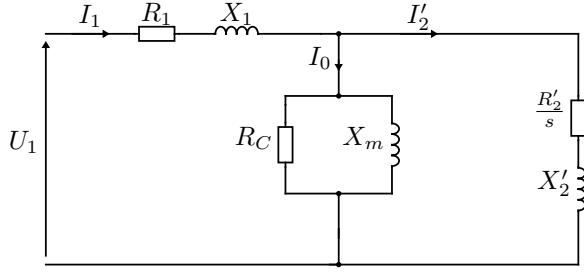


FIGURE 4: A simplified equivalent circuit of a DLIM. [21]

This induced magnetic field, and thus the primary itself, will inevitably lag behind the synchronous speed to ensure a continuous thrust force forward. Like a RIM, a LIM has a slip  $s$  that can be calculated using (3)

$$s = 1 - \frac{v}{v_s} \quad (3)$$

where  $v$  is the speed of the primary.

While there are many ways to calculate the Lorentz force induced in the secondary, a trivial way is using the motor's equivalent circuit, drawn in Figure 4. This equivalent circuit is identical to an equivalent circuit used for a RIM, as the theory is similar. The equivalent to the LIM's thrust force in a conventional IM is the torque, which can be calculated using the power created in the air gap  $P_{ag}$ , shown in (4).

$$T = \frac{P_{ag}}{\omega_s} = \frac{3 \cdot I_2' \cdot R_2'/s}{\omega_s} \quad (4)$$

Replacing the synchronous angular speed  $\omega_s$  with the synchronous linear speed  $v_s$ , the thrust force is obtained using (5).

$$F = \frac{3 \cdot I_2' \cdot R_2'/s}{v_s} \quad (5)$$

The mechanical power can be calculated by accounting for the slip, resulting in (6).

$$P_{mech} = (1 - s)P_{ag} = F \cdot v \quad (6)$$

The efficiency can be found based on the input power fed into the machine. The formula for this input power depends on whether the power is being calculated at each time step or using the RMS value of the current and the voltage. For instantaneous value, the power can be calculated using (7), whilst, with RMS values, power can be calculated using (8).

$$P_{in}(t) = 3 \cdot u_1(t) \cdot i_1(t) \quad (7)$$

$$P_{in} = S \cdot \cos(\phi) = 3 \cdot U_1 \cdot I_1 \cdot \cos(\phi) \quad (8)$$

When the input power is found, the efficiency can be calculated using (9).

$$\eta = \frac{P_{mech}}{P_{in}} \quad (9)$$

The equivalent circuit shows that the air gap power is never higher than the inserted power. As a result, there is a constraint on the efficiency, demonstrated in (10).

$$\eta < 1 - s \quad (10)$$

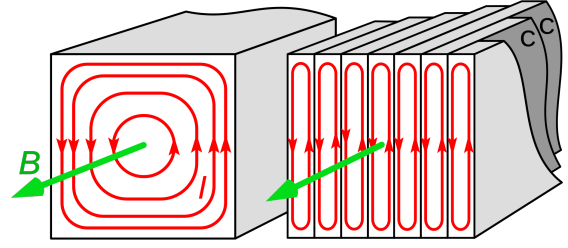


FIGURE 5: An example of laminating the motor to minimize the active flux area and thus reduce the eddy currents. [23]

Typically, the slip in LIMs is at least 10-20% [7], making the efficiency of LIMs far lower than conventional IMs.

1) *Losses in an LIM:* As the efficiency is expected to be far lower in a LIM compared to a conventional motor, there are heavy losses present in the system. These losses will be dissipated as heat, primarily in the iron core surrounding the wires in the primary. From the perspective of the equivalent circuit, the branch parameters in the core are thus expected to be relatively small compared to a RIM, meaning that more current will pass through the core, increasing the losses because of Ohm's law, see (11).

$$P = RI^2 \quad (11)$$

In a RIM, a narrow air gap and a heavy iron core result in  $R_C$  and  $X_m$  being significantly larger and thus core losses are minimal compared to what was expected in the simulations in this thesis.

In addition to the losses caused by the high air gap, the core itself will inevitably have some internal losses of its own. The core losses are typically divided into hysteresis losses, eddy current losses, and external eddy current losses. All of these losses can be derived using Steinmetz's equation, shown in (12)

$$P_{loss} = k f^a \hat{B}_m^c \quad (12)$$

where  $a$ ,  $k$ , and  $c$  are dependent on the loss type, and must be found based on curve fitting for a hysteresis loop. This is rather difficult to do, with studies dedicated solely to find these constants [22]. As such, exact calculations are beyond the scope of this thesis, but it is important to remember they are prevalent. However, eddy current losses can be minimized by cutting the core in ferromagnetic sheets and laminating them to shrink the active area, shown in Figure 5.

$$P_{cu} = R_{cu} I_1^2 = R_1 I_1^2 \quad (13)$$

In addition, copper losses will also be prevalent, with the equation shown in (13). However, none of these losses are expected to be dominant due to the high losses the larger air gap results in.

2) *Force-speed characteristics and the relation to slip:* For any IM, the torque-speed characteristics are an important aspect of the theory. An example of such a torque-speed characteristic is shown in Figure 6. Most IMs used today are



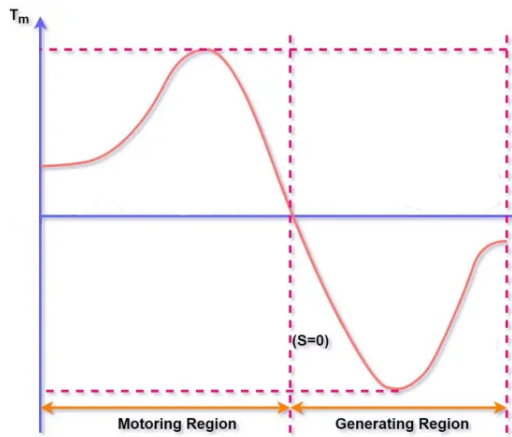


FIGURE 6: A traditional torque-speed curve of a IM. [24]

designed with a particular operation in mind, i.e. they are either generators or motors, allowing producers to optimize for the best power and efficiency around a particular point of this curve. But for a transportation system like HTS, the IM should be designed with both motor and generator purposes in mind. As such, analyzing the torque-speed characteristics, or when it comes to the LIM, the *force-speed characteristics*, is especially important.

In Figure 6, the zero point is when the machine rotational speed is set to its synchronous speed, i.e. when the machine is in a *no-load* condition. This means that the slip  $s = 0$ , and so any value to the left of this point means the machine is in motor operation, and any value to the right means the machine is in generator operation. For propulsing a LIM, the machine needs to be in motor operation, whilst when breaking a LIM, the machine needs to be in generator operation. Whilst this thesis mostly focused on the machine's motor operation, it is important to keep in mind that any LIM designed for HTS needs to be able to run in both operation regions.

It is also important to note that any IM's max torque/thrust force on a torque-/force-speed characteristic does not coincide with the motor's maximum efficiency. For a conventional RIM, the best efficiency usually sits in the region of a 2-10% slip, i.e. very close to the zero point. The maximum torque usually corresponds to a slip of 30-40% (this point is called  $T_m$  in Figure 6). A LIM has a force-speed characteristic that is similar, with maximum thrust force and maximum efficiency generally not occurring at the same speed. The difference is that the slip is usually at least 10% in normal motor operation for a LIM as mentioned in Section II-C, meaning that the best efficiency is in the 10-20% region. Like a RIM, operating the LIM for maximum efficiency is generally considered the best, as it minimizes power usage. However, it is also important that a LIM for HTS has a high thrust force to accelerate sufficiently. As such, a trade-off between these operating points might be needed.

To ensure a satisfactory operation of the LIM, it is clear that

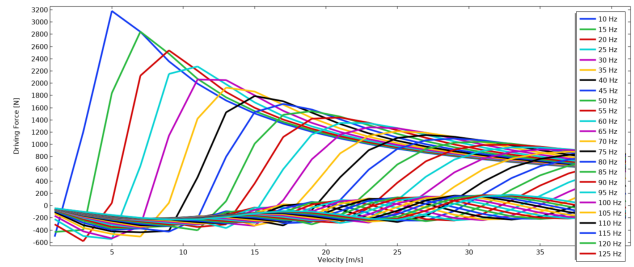


FIGURE 7: Figure from a previous study demonstrating force versus velocity for different frequencies. As the frequency increases, the maximum thrust force for a given frequency occurs at a higher speed, ensuring a continuous high thrust. [16].

the motor needs to be fed with a frequency-changing source. If the motor was fed with only one frequency for all speeds, this frequency would need to correspond to a synchronous speed higher than any speed the motor would use in normal operation to keep the LIM in motor mode. If the LIM supports HTS that can achieve speeds up to 1200 km/h, this would make the efficiency exceedingly low at start-up, as the slip would be close to 100%, making for an unsustainable propulsion system. As a result, to achieve the best possible efficiency and/or thrust force for a wide range of speeds, the motor needs to be fed with a frequency-changing source. This means that when the frequency is increased, the max thrust force is moved further to the right on the force-speed curve. An example of this from a previous study is shown in Figure 7. When the frequency is changed, so is the synchronous speed, as demonstrated by (2). A frequency-changing source is also crucial for allowing the motor to decelerate by forcing the motor to the generating region by reducing the synchronous speed. To summarize, when accelerating the motor, the motor needs to run on *ascending* frequencies, whilst when decelerating, the motor needs to run on *descending* frequencies.

3) *Finding the parameters in the equivalent circuit:* To find the parameters in the equivalent circuit, stationary simulations can be done with conditions resembling parameter tests on real-life motors. The motor's primary resistance  $R_1$  can be found by applying a DC source and measuring the resulting voltage.

$$R_1 = \frac{U_{DC}}{I_{DC}} \quad (14)$$

The secondary parameters can be found by performing a locked rotor test. In this case, the slip is 100% and can be compared to a short-circuit test of a transformer. However, this assumes that the parameters in the magnetizing branch are so large compared to the rotor branch that they can effectively be ignored. Repeated testing of induction machines throughout the years has shown that the magnetizing reactance  $X_m$  of an IM is much lower than the transformer counterpart [25]. This will have an impact on the measured resistance, and so the calculations for finding  $R'_2$  need to account for this. This results in (15) and (16).

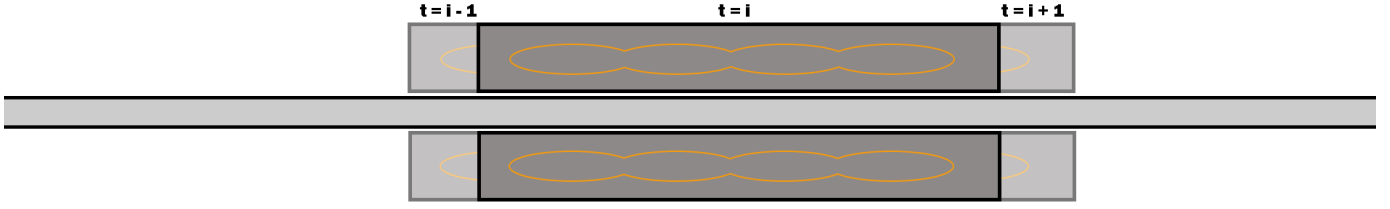
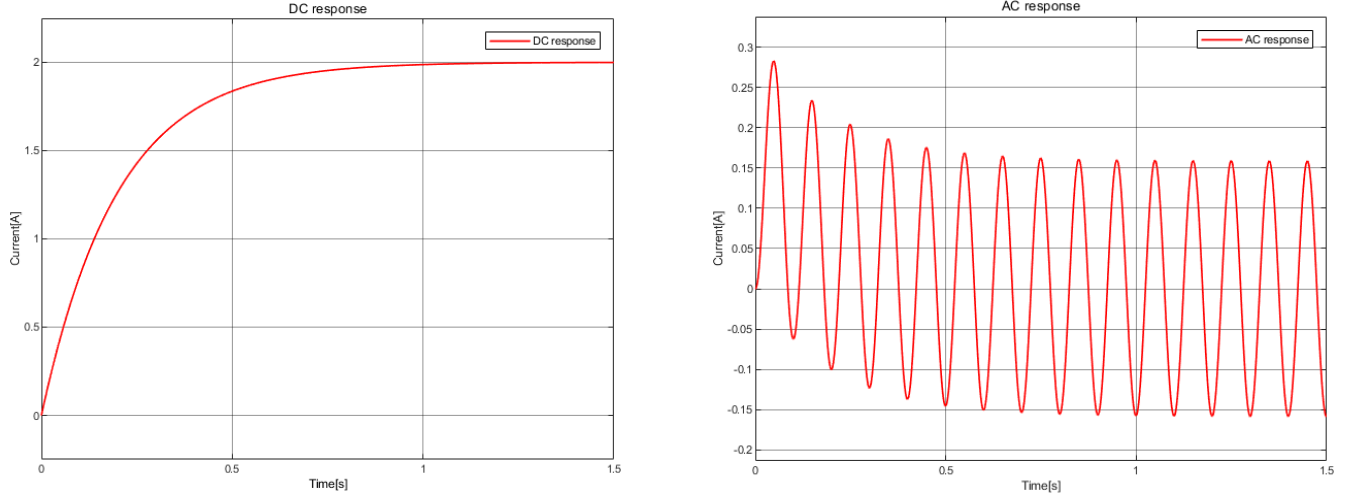


**FIGURE 8:** Bird's eye view of the DLIM moving along the secondary for each time step  $t$ .



**(A)** DC voltage source of 10 V

**(B)** AC voltage source of 10 V RMS and frequency of 10 Hz.

**FIGURE 9:** Example of an RL-circuit response with a DC and AC voltage source, respectively. The resistance is  $5\ \Omega$  and the inductance is 1 H.

$$R_{measured} = R_1 + R_2' \cdot \left( \frac{X_m}{X_m + X_2'} \right)^2 \quad (15)$$

$$X_{measured} = X_1 + X_2' \quad (16)$$

With  $R_1$  calculated,  $R_2'$  can be found using (15) and results from the following no-load test. Unfortunately, the relation of  $X_1$  and  $X_2'$  is impossible to determine based on these measurements. However, there is a consensus that these are equal in value for most motors, i.e.  $X_1 = X_2' = X_{measured}/2$  [25].

The core parameters can be found using a no-load test. The LIM can be characterized as having a no-load condition when the thrust force applied on the secondary is 0. When the thrust force is 0, the slip is at 0%, meaning that the secondary branches can be converted to an open circuit, and all currents are running through the core ( $I_{source} = I_0$ ). As with the locked rotor test, the impedance can then be found based on Ohm's law. With some circuit calculations, the core branches can be found using these formulas for  $R_C$  and  $X_m$ :

$$R_{measured} = R_1 + \frac{R_C \cdot X_m^2}{R_C^2 + X_m^2} \quad (17)$$

$$X_{measured} = X_1 + \frac{R_C^2 \cdot X_m}{R_C^2 + X_m^2} \quad (18)$$

With  $R_1$  and  $X_1$  already determined,  $R_C$  and  $X_m$  can be found using (17) and (18).

It is important to remember that the parameters in the equivalent circuit are just an approximation to analyze the motor's performance analytically. In reality, this equivalent circuit does not exist. Apart from the primary coil's resistance and reactance, the parameters in this circuit are not equivalent to coils and are not expected to behave as such. It is more likely that these values will change for any simulation test point. Again, this is not a problem if the motor is designed for a particular operating point like most IMs are, but as mentioned in Section II-C2, the motor will be used for a wide range of frequencies and speeds. Parasitic capacitances and inductances are also expected to have an influence when the motor reaches very high frequencies [26].

#### D. Computational Time-dependent Analysis in COMSOL 6

For the most part, LIMs have been simulated stationary, with some software allowing for parametric sweeps for speeds and source frequencies. However, the recent breakthroughs in FEA software like COMSOL have allowed for more transient

analysis. In particular, the release of COMSOL 6 in late 2021 allowed for linear moving mesh in addition to rotary. As a result, a time-dependent study can be done with a LIM moving along an aluminum beam at a fixed distance for each time step. This is demonstrated in Figure 8.

Compared with previous stationary analyses, a time-dependent study has both its advantages and drawbacks. A drawback is the increase in computation time. In general, time-dependent studies need to be tested over a sufficiently big simulation period to account for a time response of the motor, caused by the motor's large inductance. A simple demonstration of this is shown in Figure 9.

In addition, the sinusoidal currents applied result in a constantly changing flux in the motor, particularly in the air gap, which needs a fine mesh to be calculated accurately. To avoid interpolation, the motor needs to move at one meshed element per time step. The small time step size and relatively large simulation period results in a large number of time steps. By comparison, stationary studies need only one computation per frequency and speed to compute the values. As such, the parameters of a motor can be found in a shorter time using stationary analysis. The need for simulating motors over many speeds and frequencies as discussed in Section II-C2 also highlights the need for short computation time.

That being said, the computational abilities used in the stationary analysis have no real-life comparison. In stationary analysis, a Lorentz force is calculated based on the flux passing through and currents induced in the motor's secondary. These currents and fluxes can never be measured in practice, making the results of stationary analysis hard to interpret. However, the time-dependent analysis does have a real-life comparison, as moving a built motor along an aluminum rail with a constant speed can be considered a realistic test of a motor. In other words, the results derived from transient simulations should be valuable, as they can interpret the meaning of the results found in stationary analysis, whilst highlighting the shortcomings of it and the advantages of transient simulations.

### III. METHOD FOR ANALYSIS

#### A. Building the model

1) *Simulation Domain:* The simulation domain was built in a COMSOL 2D model using the parameters shown in Table I, and fitting materials were selected. The dimensions were based on a previous model developed last year in [17], where a DLIM was mounted on an aluminum beam with a surrounding air domain. However, some changes had to be made since the new model would also be used for transient analysis. Firstly, the aluminum beam and the air domain surrounding the motor were reduced. Reducing the air domain was especially important, as it would move along with the motor in time-dependent simulations. Ideally, the motor would have moved alone with air as a background domain. Unfortunately, moving objects in COMSOL can only move onto empty domains, meaning that the motor and surrounding air would have to be moved together. Moving meshed objects is also computationally demanding to calculate, and if this surrounding air domain

**TABLE I:** Parameters for the DLIM inserted into FEA-software.

Name	Description	Value
$I$	Phase current	70 A
$m$	Number of phases	3
$N$	Number of winding turns	10
$J$	Current density	$8 \frac{\text{A}}{\text{mm}}$
$FF$	Fill factor	0.5
$2p$	Number of poles per phase	8
$\tau_p$	Pole pitch	55.25 mm
$\sigma_{Cu}$	Copper conductivity	$5.998 \times 10^7 \frac{\text{S}}{\text{m}}$
$\sigma_{Al}$	Aluminium conductivity	$3.030 \times 10^7 \frac{\text{S}}{\text{m}}$
$h_{air}$	Air domain margin height (surrounding the LIM)	0.03 m
$w_{air}$	Air domain margin width (surrounding the LIM)	0.02 m
$2a$	Model depth	100 mm
$L_{LIM}$	LIM length	442 mm
$h_{LIM}$	LIM height(back iron)	20 mm
$w_t$	Tooth width	10 mm
$w_s$	Slot width	8 mm
$h_s$	Slot height	15 mm
$L_{Al}$	Secondary(rail) length	2 m
$h_{Al}$	Secondary(rail) thickness	4 mm
$g$	Air gap	2mm
$f$	Source frequency	Chosen for simulation
$v$	LIM velocity	Chosen for simulation

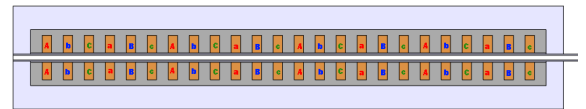


**FIGURE 10:** Full view of the LIM built-in COMSOL for the simulation. The winding distribution is shown with a, b, and c. Small letters mean the currents are flowing in the reverse direction.

was large, this would result in infeasible computation time. As such, a smaller air domain surrounding the motor made for sufficiently short computation time, whilst realistically simulating the leakage flux a LIM makes to the surrounding air.

2) *The motor model:* The LIM model had a simple design, with dimensions that could realistically be implemented for the HTS, while not being too large for infeasible computation time. The goal of the motor design was to make the motor as

basic as possible to highlight the characteristics of a LIM and to compare it with the theoretical background, not to perfect the performance.

The copper windings used a standard anti-periodic layout, shown in Figure 10. Since this was a 2D model, the end windings of the copper coil were not possible to implement and were as such neglected. While this made the model inaccurate, the heavy reduction in computation time made 2D modeling the better option compared to 3D. Additionally, the same coil was applied to both sides of the motor in this layout. In a realistic implementation, this would mean that the motor was series connected across at one end of the motors, requiring only one three-phase source. The iron yoke was dimensioned with concerns to the distribution and flow of the magnetic field, and as with the rest of the iron core, was selected with a B-H curve to account for magnetic field saturation, as well as the expected core losses. The electric conductivity of the iron core was set to zero to account for lamination.

The parameters and material chosen resulted in the model presented in Figure 11, where the air domain is shown in a light blue color surrounding the motor. Geometric domains of the LIM are further highlighted in Figure 12. A small air gap surrounded the aluminum rail in addition to the moving air gap in the LIM to make the simulation more dynamic. This can be seen better in Figure 13. Using the assembly tool, a boundary was created between the motor and the aluminum rail, which allowed the motor to move along the rail using moving mesh. With this setup, stationary and time-dependent analysis could be performed on the same model, allowing for a direct comparison of results. However, there were some differences when simulating. Apart from the obvious time dependency, the currents applied in the stationary analysis were applied using complex numbers, shown in (19). This form produces the best results, as important parameters such as power factor and apparent power can easily be calculated. Unfortunately, this form produces non-converging results when doing a time-dependent analysis, so the currents applied in this case used trigonometric functions, shown in (20). While these two forms are equivalent in theory, some approximation errors were to be expected with computational software. Other differences when simulating are explained in Appendix Section A.

$$I = I_{max} \cdot e^{a \cdot j \cdot \frac{2\pi}{3}}, a = 0, 1, 2 \quad (19)$$

$$i(t) = I_{max} \cdot \cos(2\pi f \cdot t - a \cdot \frac{2\pi}{3}), a = 0, 1, 2 \quad (20)$$

The meshing of the motor is shown in Figure 14. The total number of FEA elements was 72652. The motor was finely meshed, particularly in the air gap and the aluminum beam to account for the exchanging flux penetrating the beam between the motor halves. The number of elements in the air gap was chosen as 3000, resulting in 0.667 mm distance between the nodes. As discussed in Section II-D, the motor needed to move one mesh-element per time step to avoid interpolation in transient results, meaning the LIM moved 0.667 mm per time

step. This resulted in a significant number of time steps and the motor was thus simulated over only a few electric periods to make the simulation time feasible. In this case, 4 electrical periods were selected for all simulations, resulting in 450 time steps per transient simulation.

3) *Initial conditions:* The initial conditions were set to zero for the time-dependent analysis. This means that the motor is instantly accelerated to the given speed, while it is also applied a sinusoidal three-phase current at the same time. This would likely result in an overshoot of the thrust force, and by extension the efficiency, especially when this speed is high. In a real implementation, the motor would be gradually accelerating to a given speed. For the simulation to be more realistic, a different initial condition could have been set for the motor. However, what this initial condition should have been for each speed was hard to determine, as COMSOL can only give the initial condition for the magnetic vector potential, and not a given speed or thrust force. As such, with initial conditions set to zero, initial errors were expected, but it resulted in more predictable results. In addition, these errors were likely to correct themselves over time.

4) *Analytical results:* The analytical results could be obtained in many ways. One of the more trivial ways was to use the equivalent circuit provided in Figure 4 and recreate it using Simulink. Figure 15 shows this model. The equivalent circuit was duplicated twice to account for a three-phase system, with the power sources 120° phase shifted from each other. Unlike COMSOL, which applies current in coils, the Simulink model used voltage sources. As such, the magnitude of the voltage, as well as the rest of the parameters of this circuit, were found based on computational results in COMSOL's stationary analysis. As discussed in Section II-C3, the parameters were expected to change when adjusting the operational frequency. To keep the analytical results closer to the results from the FEA, they were updated for each new operating frequency. In a normal circuit, branch parameters would not change with different frequencies. However, as also mentioned in Section II-C3, this equivalent circuit does not exist in reality, making this change justifiable. Applying a voltage and a given slip to this circuit resulted in a time-dependent simulation. However, due to the simplicity of the computations, they were not expected to have a behavior similar to the time-dependent simulations done in COMSOL.

## B. Finding the losses

For analytical results, the equivalent circuit shows that the core parameters account for the core losses, and the air gap power not converted to mechanical power is considered as air gap losses. As such, separating core losses in analytical results is trivial. However, as mentioned in Section II-C3, this equivalent circuit is not real, and therefore it might have been unreasonable to separate loss types by using a tool that was there to calculate simple parameters such as thrust force and efficiency, but not for detailed study.

As such, FEA was probably the best way to understand where the losses in the motor occurred. However, to do this,

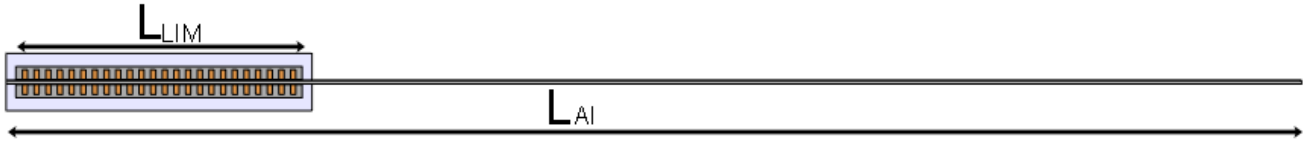


**FIGURE 11:** The domain used for simulation. A DLIM is connected to a 2-meter-long aluminum rail. Geometric dimensions are highlighted.

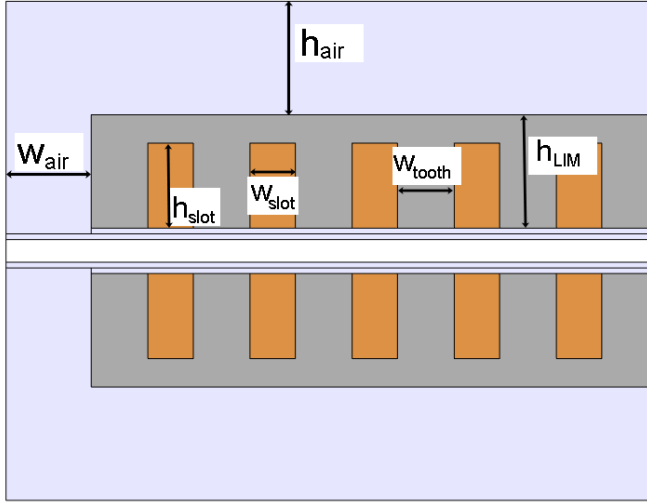


**FIGURE 12:** Medium close-up of the domain used for simulation, highlighting the geometric parameters for the LIM.

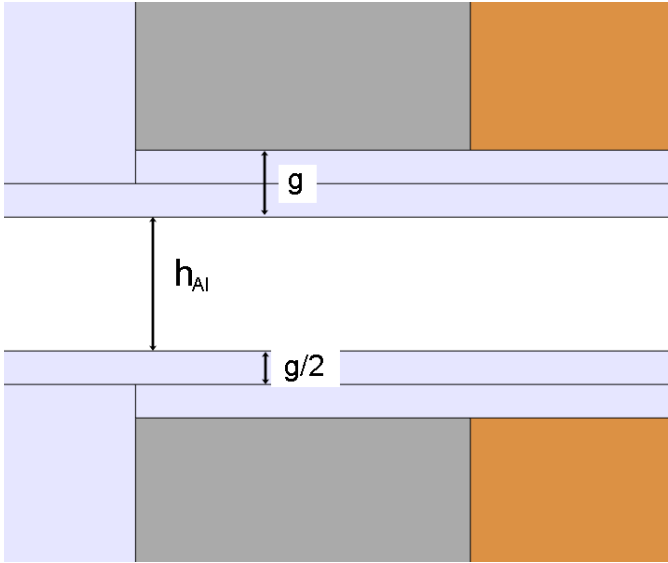


**FIGURE 13:** Close-up of the LIM designed for the simulations, highlighting the air gap on the LIM as well as on the aluminum beam.

heat studies were needed. This required applying a different set of physics and studies, which would have been time-consuming. The simulations that were needed for this thesis were also considered time-consuming. As such, separating the power losses was beyond the scope of this thesis, except

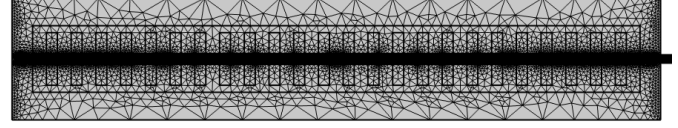


**FIGURE 14:** Screenshot of the mesh used for the simulations. The total number of elements for the entire domain was 72652. The total number of nodes in the air gap along the beam was 3000, resulting in 0.667 mm distance between the nodes.

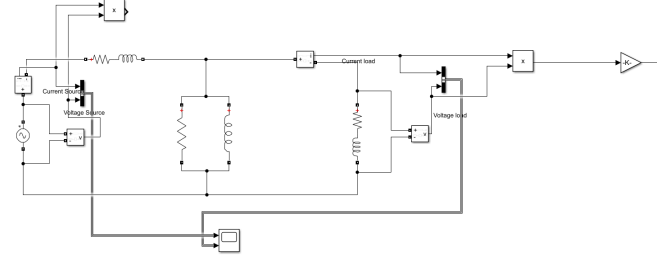


**FIGURE 15:** Simulink model of the equivalent circuit.

copper losses, which could be calculated using (13).

### C. Choosing a simulation point

When choosing a simulation point for study purposes, i.e. selecting a particular speed for a particular frequency, it is natural to assume that one should pick the point with the best efficiency and the best thrust force. However, as mentioned in Section II-C2, these points do usually not coincide, and as such a trade-off between the two needed to be analyzed. In general, selecting the point with the best efficiency is preferred, to minimize power usage. That being said, thrust force rapidly declines with increasing operating speed near the synchronous speed, as shown in Figure 6. For LIM, a motor type that is considered to have a lower propulsion than conventional IMs, it might be needed to optimize for a sustainable thrust force at the cost of lower efficiency.

When a speed was selected, the operating voltage could be obtained from stationary results and inserted into the equivalent circuit. The slip could also be calculated and inserted using the  $\frac{R'_2}{s}$  parameter. Note that the theoretical synchronous speed might not coincide with the speed where the thrust force  $F = 0$  for stationary analysis, as computational approaches are more complex than analytical formulas. To make the analytical results as close to theory as possible, the synchronous speed from (2) was chosen if the speeds did not match.

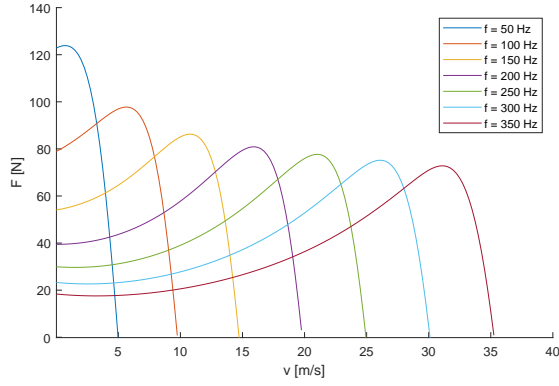


**FIGURE 16:** Force-speed characteristic of the 2D LIM model for stationary simulations in the frequency plane at the frequencies selected for the simulations.

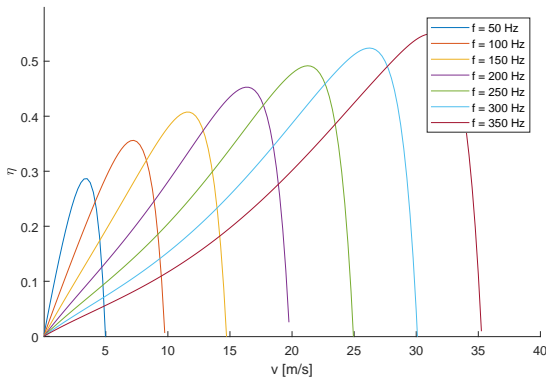


**FIGURE 17:** Efficiency-speed characteristic of the 2D LIM model for stationary simulations in the frequency plane at the frequencies selected for the simulations.

## IV. RESULTS

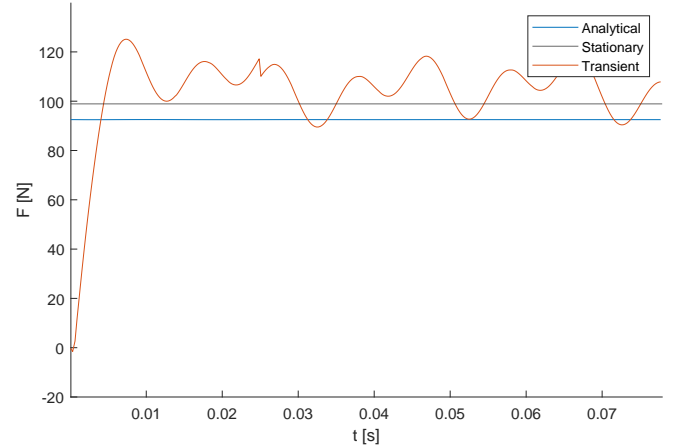
### A. Force-speed characteristics

Figure 16 and Figure 17 show the force-speed characteristic and the efficiency-speed characteristic of the motor respectively. The figures show that the highest thrust force decreased with ascending frequency. The efficiency, on the other hand, increased with ascending frequency. They also show that the motor's no-load condition occurred at a lower frequency than the theoretical synchronous speed. E.g. the motor's no-load at 150 Hz occurred at 14.7 m/s, while the motor's theoretical synchronous speed at this time was 16.575 m/s, an 11% difference. This difference stayed about the same for all frequencies. However, as mentioned in Section III-C, the theoretical synchronous speed would be chosen for finding the analytical results.

The raw data from Figure 16 and Figure 17 were used to find an optimal operating point for each frequency based on the maximum torque and efficiency. As expected, these points did not always align, as such a trade-off between the points was made. Finally, the optimal operating speed for each frequency is shown in Table II. The voltages for the operating points, along with the rest of the critical parameters are shown in

**TABLE II:** Operating speeds chosen for the transient and analytical results based on the characteristics of the motor. Chosen as a trade off between maximum thrust force and maximum efficiency.

Frequency[Hz]	Operating speed[m/s]
50	3
100	7.25
150	11.5
200	16.25
250	21.25
300	26.25
350	31



**FIGURE 18:** Thrust force on the aluminum beam for  $f = 50$  Hz and  $v = 3$  m/s. The transient results are from the 2D LIM model simulated in a time-dependent moving-mesh study over 4 electrical periods. The sudden drop for transient results around  $t = 0.025$  s was a computational error.

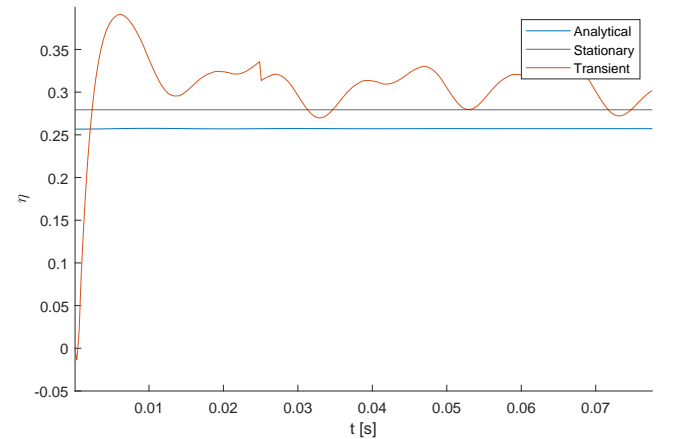


**FIGURE 19:** Efficiency of the LIM for  $f = 50$  Hz and  $v = 3$  m/s. The transient results are from the 2D LIM model simulated in a time-dependent moving-mesh study over 4 electrical periods. The sudden drop for transient results around  $t = 0.025$  s was a computational error.

Appendix Section B. Using these operating points, transient and analytical simulations could be done by inserting the speed for the given frequency.

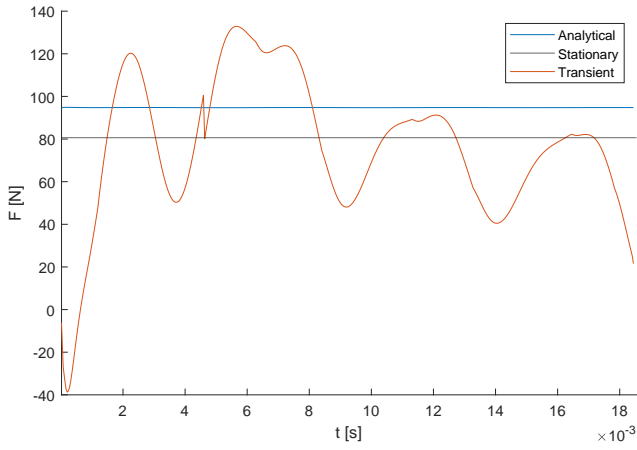


**FIGURE 20:** Thrust force on the aluminum beam for  $f = 200$  Hz and  $v = 16.25$  m/s. The transient results are from the 2D LIM model simulated in a time-dependent moving-mesh study over 4 electrical periods. The sudden drop for transient results around  $t = 0.005$  s is a computational error.

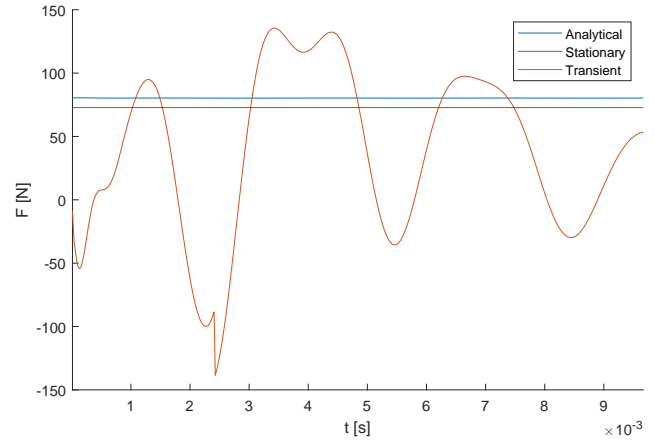


**FIGURE 22:** Thrust force on the aluminum beam for  $f = 350$  Hz and  $v = 31$  m/s. The transient results are from the 2D LIM model simulated in a time-dependent moving-mesh study over 4 electrical periods. The sudden drop for transient results around  $t = 0.0022$  s and at the end was a computational error.

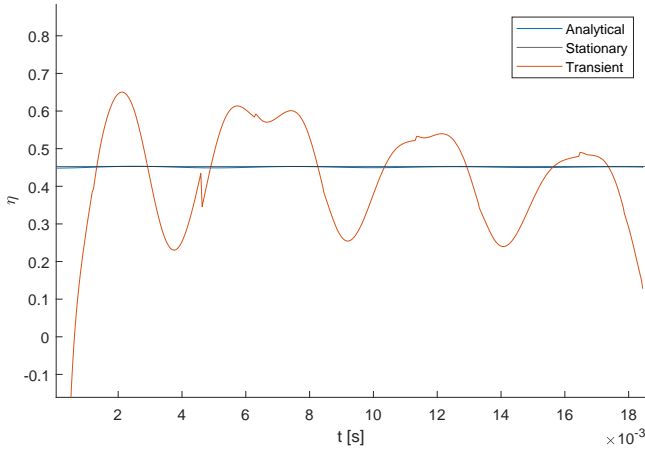


**FIGURE 21:** Efficiency of the LIM for  $f = 200$  Hz and  $v = 16.25$  m/s. The transient results are from the 2D LIM model simulated in a time-dependent moving-mesh study over 4 electrical periods. The sudden drop for transient results around  $t = 0.005$  s was a computational error.

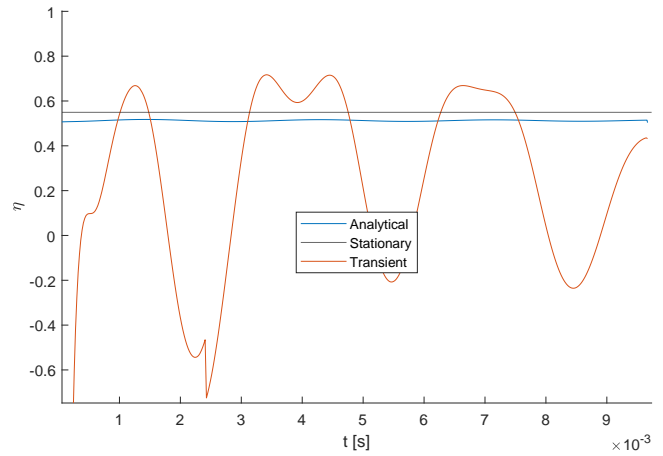


**FIGURE 23:** Efficiency of the LIM for  $f = 350$  Hz and  $v = 31$  m/s. The transient results are from the 2D LIM model simulated in a time-dependent moving-mesh study over 4 electrical periods. The sudden drop for transient results around  $t = 0.0022$  s and at the end was a computational error.

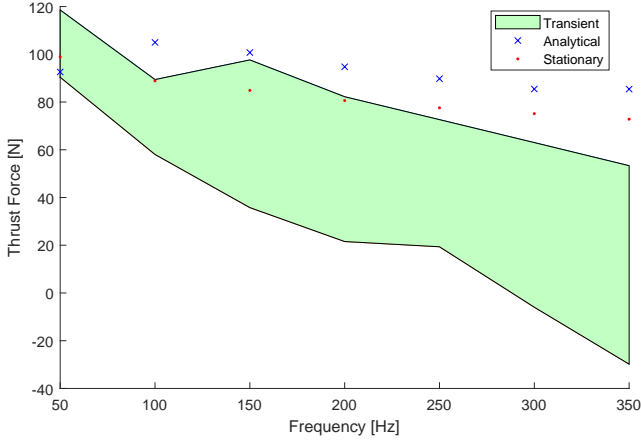
### B. Results for optimal operating points

Figure 18 and Figure 19 show the thrust force and efficiency, respectively, for the first operating point. Notice that around  $t = 0.25$  s, there is a sudden drop in the results for transient analysis. This was due to a computational error and as such is not linked to any real behavior of a LIM. The error was likely caused by the uneven mesh at the end of the motor, as this error happened when the DLIM had moved the length of itself along the rail. This computational error was present at all of the simulations, though at different times since the motor moved faster for higher frequencies.

The results show that there was coordination between the analytical and stationary results, particularly in efficiency. The transient results also tended towards analytical and stationary results. However, as the speed elevated, the initial step response in the transient results became larger and larger. This

step response can be observed in Figure 20-23.

Looking at the transient results, it is hard to ignore the significant ripple in thrust force and efficiency. Assuming the stationary results acted as some middle point for  $f = 50$  Hz in Figure 18, the ripple was at 20%. This is high compared to conventional IMs, and the ripple only became larger with higher speeds. However, there are some reasons why the ripple shown in the figures for higher speeds might not have been accurate. The thrust force over time in Figure 22 shows that the motor transitioned to generator mode after the initial peak. This is confirmed in Figure 23, as the efficiency calculated using (9) became nonsensical as the generating power was higher than the supplied power. As this is an operating speed within the motor operation area, this was likely also part of the step response of the motor.



**FIGURE 24:** Collected diagram of the thrust force for transient, analytical, and stationary results for all frequencies. The analytical results contain the final value of the thrust force of the simulation in Simulink. Stationary and transient results are from the 2D FEA LIM model. Stationary results are the single value output from the stationary study in the frequency plane. The transient results are from the time-dependent study over 4 electrical periods and its uncertainty region's maximum and minimum points are the top and bottom of the last wave of the simulation.

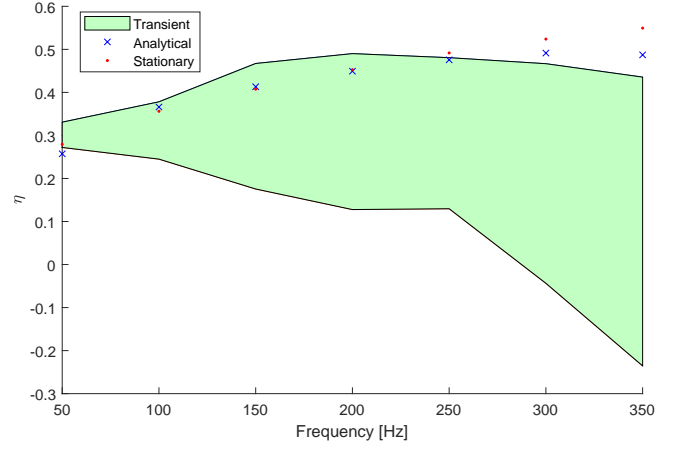


**FIGURE 25:** Collected diagram of the efficiency for transient, analytical, and stationary results for all frequencies. The analytical results contain the final value of the efficiency of the simulation in Simulink. Stationary and transient results are from the 2D FEA LIM model. Stationary results are the single value output from the stationary study in the frequency plane. The transient results are from the time-dependent study over 4 electrical periods and its uncertainty region's maximum and minimum points are the top and bottom of the last wave of the simulation.

Other results showing the same trend for the rest of the frequencies can be found in Appendix Section C.

### C. Comparing the results for all frequencies

The collected results for thrust force and efficiency are shown in Figure 24 and Figure 25, respectively. The figures show that the analytical computations aligned closely with the results from the stationary simulation. The transient results were in comparison extremely uncertain. However, the transient results seem to suggest that the stationary results were the maximum value of what could be obtained, as the maximum thrust force and efficiency from the transient results were close to the stationary values.

### D. Power loss in the LIM

By combining the results of efficiency and thrust force, the total losses could be obtained, shown in Figure 26. Like expected, the losses were substantial, likely resulting in significant heat development in the system. The copper losses were constant and minimal compared with the total losses.

### E. Edge effects

Figure 27 and Figure 28 show the edge effects of the LIM tested for  $f = 300$  Hz and  $v = 26.25$  m/s. Figure 29 and Figure 30 show the same effects for the stationary simulations. The edge effects were present at this speed, with little flux exchange in the entry, and considerable flux exchange after the motor had left the beam. Note that the end effects in Figure 28 and Figure 30 had a strong point at the edge of the air domain. This is because the small air domain concentrated the field lines at this point. If the air domain was bigger, the end effect would have been more distributed. Nevertheless, since what impacts a motor performance is the end effect itself, not the distribution, simulation domain changes were not needed.

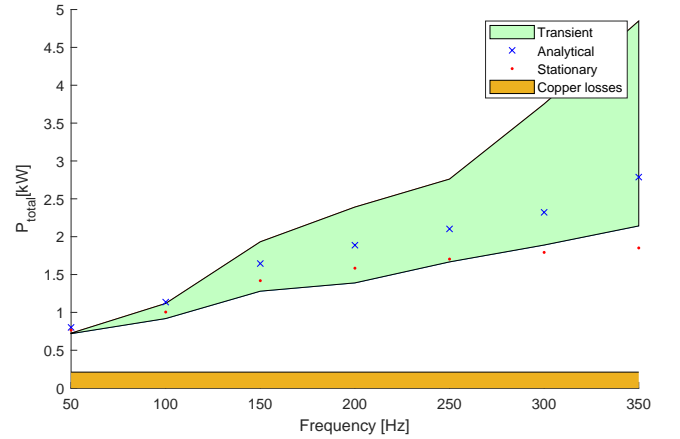


**FIGURE 26:** Collected diagram of the losses for transient, analytical, and stationary results for all frequencies. The analytical results contain the final value of the power loss of the simulation in Simulink. Stationary and transient results are from the 2D FEA LIM model. Stationary results are the single value output from the stationary study in the frequency plane. The transient results are from the time-dependent study over 4 electrical periods and its uncertainty region's maximum and minimum points are the top and bottom of the last wave of the simulation. Copper losses for all three simulation types are the same.

## V. DISCUSSION

### A. Difference in synchronous speed

Upon further inspection of Figure 16 and Figure 17, there was a 9-11% difference in the synchronous speed between the theoretical formula and the stationary results. Such a difference perfectly highlights the shortcomings of transferring theory from RIMs to LIMs. Looking at (2), the equation is a copy of (1) adjusted for linear motion. In a RIM, the electromagnetic field is running constantly within the iron core in the stator,



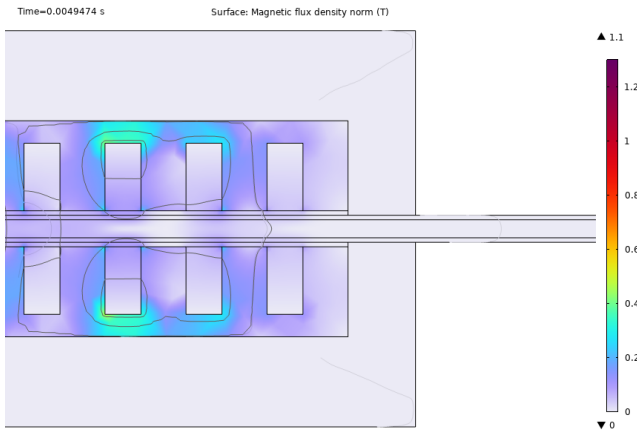


**FIGURE 27:** Right side of LIM demonstrating entry effect. Taken from the transient simulation of  $f = 300$  Hz and  $v = 26.25$  m/s. Screenshot from COMSOL.

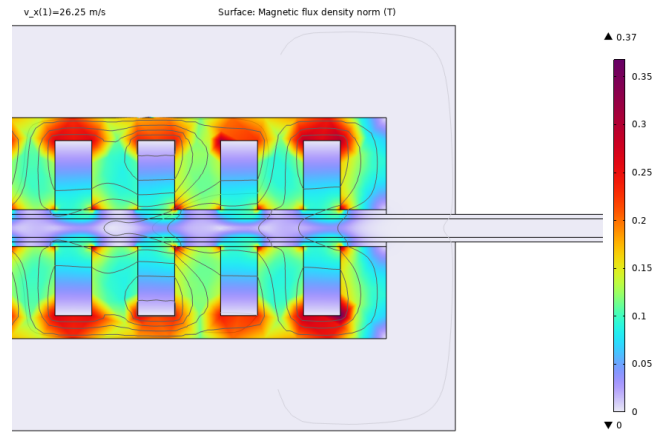


**FIGURE 29:** Right side of LIM demonstrating entry effect. Taken from the stationary simulation of  $f = 300$  Hz and  $v = 26.25$  m/s. Screenshot from COMSOL.

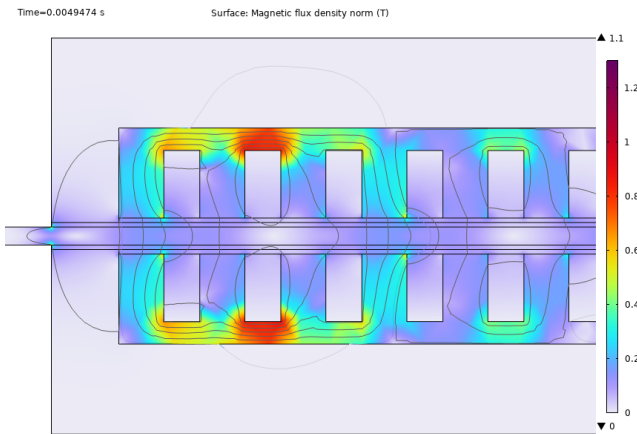


**FIGURE 28:** Left side of LIM demonstrating end effect. Taken from the transient simulation of  $f = 300$  Hz and  $v = 26.25$  m/s. Screenshot from COMSOL.

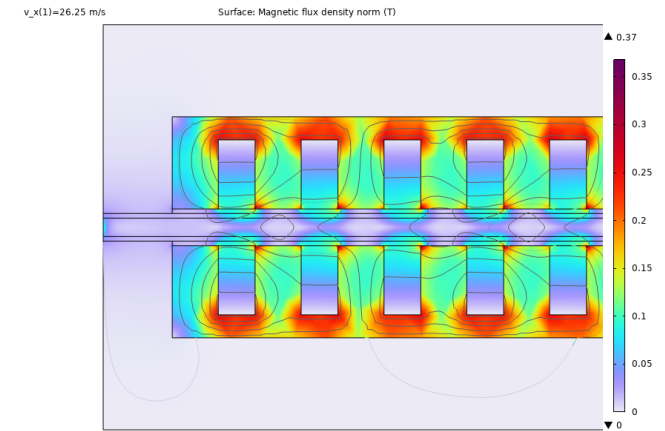


**FIGURE 30:** Left side of LIM demonstrating end effect. Taken from the stationary simulation of  $f = 300$  Hz and  $v = 26.25$  m/s. Screenshot from COMSOL.

ensuring continuous conduction of the magnetic field and making (1) a rational approximation.

A continuous electromagnetic field conduction also means that the no-load test for a RIM does happen at the theoretical synchronous speed. For this to happen in a LIM, the primary and secondary would have to be infinitely long. Naturally, the motor simulated was far from that, and as a result, the electromagnetic wave created in the primary was not conducted in an iron core all the time. This resulted in the no-load condition happening at 9-11% theoretical slip instead of 0%. As a result, using theoretical slip as a constraint for efficiency is arguably not fair to a LIM, as it is practically impossible for the no-load condition to happen at the same speed as a RIM. However, (10) still holds, as  $1 - s$  is a strict upper bound.

That being said, theoretical slip is still valuable when calculating thrust force and efficiency in a LIM. The analytical results found in Figure 18-25 were based on applying the theoretical slip in the  $R'_2/s$  parameter in Figure 4. If the slip

related to the real no-load condition was used, the analytical and stationary results would not have aligned so well. In other words, the results show that the theoretical slip is useful when analyzing a LIM, but it is impossible to achieve this slip using a no-load condition.

### B. The validity of transient results

Unfortunately, the large ripples from  $f = 150$  Hz – 350 Hz made the transient results difficult to interpret. Ideally, the thrust force in transient results should have had an initial ripple but approach the stationary results over time. However, the thrust force and efficiency shown in Figure 20 and Figure 21 did not seem to do this, and the ripple was too large to be sensible. As mentioned in Section IV-B, this was likely part of the step response, as the speed accelerated from 0 to a high operating speed. It is also likely that this step response had not disappeared by the end of the simulation time. In the most extreme example of  $f = 350$  Hz, the motor was only simulated for about 0.01 s, as shown in Figure 22, and considering that this motor ran at  $v = 31$  m/s  $\approx 112$  km/h,

this resulted in a severe acceleration. In addition, the currents in the coil were also triggered at the time step prior to the speed change, resulting in a step response of its own. The induced magnetic field caused by the current followed by an acceleration from 0 to 31 m/s one time-step later resulted in an extreme step response of the motor which naturally did not dissipate after  $t = 0.01$  s. The thrust force and efficiency for these frequencies may approach the stationary results, but the motor was not simulated over a sufficient period to show this. As such, a simulation time larger than the one used is needed for higher frequencies, in order to give a true reflection of the motor's thrust force and efficiency. Unfortunately, this results in infeasible computation time for this model.

### C. Thrust force

The force-speed characteristic found in Figure 16 was as expected, decreasing with ascending frequencies. The analytical results deviated from stationary results at certain frequencies but were a satisfactory match overall. The deviation might be caused by the simplifications made with the parameters found in the equivalent circuit. The relation of  $X_1 = X'_2$ , derived from a consensus after testing IMs, might not have been ideal for this motor. After all, the motor's secondary, which was what the  $X'_2$  parameter was based on, was a linear aluminum beam and not a cylindrical iron core like in a normal IM. To achieve better results, different relations could have been experimented on. That being said, an equivalent circuit will always neglect certain complexities a LIM has, such as the edge effects. As such, this equivalent circuit would likely never have a 100% equivalence with computational results, as the computational results used FEA to study the motor at a fundamental level.

The collected results for the thrust force in Figure 24 show that the ripple was significant for low speeds but increased heavily with ascending speed. However, as mentioned in Section V-B, it is difficult to interpret the results when the speed was increased, as the step response in the aluminum beam likely had not corrected itself by the end of the simulation. Nevertheless, the transient results from the lowest frequencies seem to prove the analytical and stationary results, which show that the thrust force was relatively high in the beginning. That being said, a 20% ripple is too significant for this motor to be implemented. It is not clear how much of this ripple was caused by the differences of a LIM compared to its rotary counterparts, and how much was due to a poor design. A better design would probably reduce the ripple, but how much is difficult to conclude.

### D. Efficiency

The efficiency-speed characteristic found in Figure 17 was also as expected compared to previous studies [17], increasing with ascending frequencies. The analytical results found were in many cases an even better match to the stationary results than the thrust force. Looking at the definition of efficiency in (9), this improvement was due to the relation between the input

and mechanical power staying the same. I.e. when the analytical thrust force deviated from the stationary, the input power also deviated at a similar rate, giving a near-perfect match for the efficiency. This also suggests that the deviations might not only have been caused by the simplifications regarding the circuit parameters but also by expecting the same behaviors for all three phases. Since the LIM was not infinitely long, phases at the edge of the LIM could have had a slightly different operating voltage. Looking at Figure 10, these phases were A and C. It is possible that this slight unevenness interfered with the voltages the same way as it interfered with the induced magnetic field. Using this argument, it is possible to envision that these effects canceled each other out, giving a better correspondence between analytical and stationary results.

That being said, much can be said about the efficiency that has already been said about the thrust force. Looking at Figure 18-23, the graphs for the efficiency and the thrust force have almost the same ripple. From Figure 19, a rough estimate suggests that the ripple was at 15%. This was lower than the ripple in the thrust force shown in Figure 18, meaning that there was an overlapping ripple in the input power which reduced the ripple in the efficiency. This was consistent throughout the simulations when the speed increased, as the efficiency graphs had a slightly less ripple than the thrust force for the same frequency. This further proves that the LIM had not stabilized itself, as the input power should have stayed constant if the system was stable. At higher speeds, the high thrust force ripple could have also had a generating effect on the LIM, meaning that the input power would be influenced by the mechanical power. This is especially visible in Figure 23, where the formula for efficiency at several moments became obsolete as the LIM switched to generator mode.

Nevertheless, the results for the lowest frequencies showed that efficiency was low for this design, and as such it would require significant input power to accelerate the motor from stand-still. For high speeds, while less certain, the efficiency would likely increase. Like with the thrust force, different starting conditions or a longer simulation time could confirm this.

### E. Power losses

Figure 26 show the total losses in the LIM for the frequencies and operating points tested. As explained in Section II-C1, the losses in the machine were core losses, air gap losses, and copper losses. The theory established in Section II-C1 allowed for copper losses to be calculated, and are as such shown in Figure 26 as a portion of the total losses. These losses were the same for every type of simulation, as the current applied and the copper resistance were constant for all frequencies. However, the other losses were more difficult to determine for each simulation and were not separated, as mentioned in Section III-B.

### F. Edge effects

The edge effects were prevalent in the transient results, as can be seen in Figure 27 and Figure 28. These edge effects

were also present in stationary simulations, as can be seen in Figure 29 and Figure 30. The latter figures show that the even distribution of the magnetic field in the stationary made the edge effects less consequential. By comparison, the pulsating distribution of the magnetic field in the coils shown in the transient results made the edge effects have a far bigger impact.

Looking back at the collected graphs in Figure 24 and Figure 25, stationary results seemed to act as a best-case scenario for the motor's real performance demonstrated in the transient results, especially for the higher frequencies. The near uniform distribution of the magnetic field in the stationary results further suggests that this is reasonable, as a uniform distribution is an ideal case for the best possible propulsion. As such, the edge effects could have been a reason why the motor had such a significant ripple. If so, this is surprising, since the edge effects were not expected to have a significant impact on the performance at the low frequencies tested. However, the short simulation time also means that it is uncertain how much of this ripple was caused by edge effects, as a significant portion was undoubtedly caused by the step response the motor had for higher speeds.

As mentioned in Section II-B, edge effects are expected to be more prevalent at higher speeds than those simulated in this thesis. If edge effects contributed to the ripple at the frequencies tested, the ripple will only increase when the speed is raised. As such, the motor designed might never have a stable thrust force and efficiency for higher speeds. That being said, as optimal motor design was not relevant to this thesis, it is not clear whether these edge effects are reducible with a better design, or if they are simply unavoidable.

## VI. CONCLUSION

This thesis has attempted to highlight a LIM's performance for HTS at low frequencies. Concretely, the thrust force and efficiency were chosen to quantify the performance. The system was limited to a DLIM surrounding an aluminum beam segment. Analytical results were derived by converting and adjusting the theory used for conventional IMs, including the use of an equivalent circuit inserted into Simulink. Stationary, as well as time-dependent simulations were done on a 2D model built in COMSOL, a FEA program. Results from stationary simulations were used to find the parameters in the equivalent circuit, as well as derive optimal operating points for the LIM at a given frequency.

The findings in this thesis concluded that the analytical results were generally optimistic regarding thrust force compared to stationary results, whilst coinciding very well regarding efficiency. The transient results, though inconclusive, suggested that the ripple produced in a LIM was exceedingly high. The transient results also implied that the stationary results of the thrust force and efficiency acted as a maximum for the higher frequencies tested. Edge effects might have been a reason for the large ripple, as they were shown to be prevalent throughout the transient simulations. However, initial conditions set to zero were likely the cause for the unsustainable large ripple at the higher frequencies tested, causing a significant step

response that did not disappear due to the short simulation time, albeit tended to reduce.

Based on the findings found in this thesis alone, the LIM would not be a viable option for HTS. Whilst stationary and analytical results are reasonable, the ripples present in the transient results are unacceptable to provide continuous acceleration and sustainable efficiency. However, this ripple can likely be improved, as this thesis has not aimed at perfecting the design of the motor. Additionally, 2D modeling as a constraint was not enough to reduce computation time to the amount that this thesis had, meaning that the causes of the ripple were not clarified. As such, a longer simulation time along with different initial conditions is also needed to decipher how much of this ripple is caused by the design, and what is inevitable to have on a LIM.

## VII. FUTURE WORK

The findings of this thesis suggest that these issues need to be further explored:

- The ripple in the thrust force and efficiency needs to be reduced, in particular for higher frequencies and operating speeds. Longer simulation times as well as different initial conditions will clarify a LIM's step response over time during acceleration. As such, the problems regarding the design of the LIM can be isolated, allowing for improvement of the design through trial and error. Possible improvements include changing the winding layout and dimensioning of the iron surrounding the coils, and narrowing the air gaps as much as possible whilst keeping a safe distance to avoid collisions that could happen in a realistic implementation.
- Related to finding more expansive results, is the need to minimize computation time. While attempts were made to reduce the computation time in this thesis, it is arguably too high to be sustainable for thorough analysis. Improvements can be made by further shortening the aluminum beam, segmenting the motor, or improving the mesh. The latter would also remove the computational errors present in this thesis.

## ACKNOWLEDGEMENTS

This has been a challenging process, with a steep learning curve for a relatively new concept. I would like to thank my supervisor Jonas K. Nøland for staying patient with me throughout the year, whilst providing valuable input by supplying relevant studies, and guidance in times of trial. I would also like to thank my co-students for providing relevant articles and inspiration for completing the thesis. Finally, I would like to thank my family for their moral support throughout the years, particularly this final one as my MSc has come to an end.

## REFERENCES

- [1] E.Musk, "Hyperloop Alpha" SpaceX, Hawthorne, CA, USA, Tech. Rep., 2013. Available: [https://www.tesla.com/sites/default/files/blog\\_images/hyperloop-alpha.pdf](https://www.tesla.com/sites/default/files/blog_images/hyperloop-alpha.pdf)

- [2] Gray, J.S., Decker, K., Sakib, G., Nguyen, G., Summers, C., Oberlander, A., Sharifrazi, N., Chin, J.C., Heath, C.M., Falck, R., & Peng, A. (2017). Conceptual Feasibility Study of the Hyperloop Vehicle for Next-Generation Transport.
- [3] K. Shaaban and E. Radwan, "Design Challenges for Hyperloop Transport Systems", *2022 Intermountain Engineering, Technology and Computing (IETC)*, Orem, UT, USA, 2022, pp. 1-4, doi: 10.1109/IETC54973.2022.9796713.
- [4] J. Kim, H. Kim and K. J. Han, "Hyperloop Communications: Unveiling Electromagnetic Propagation in the Hyperloop Tube," in *IEEE Vehicular Technology Magazine*, vol. 17, no. 3, pp. 65-74, Sept. 2022, doi: 10.1109/MVT.2022.3143109.
- [5] J. Dong, B. Becetti and P. Bauer, "Design of Multi-Mode Linear Electric Machine for Charging and Propulsion of Vacuum Tube Train," *2022 International Conference on Electrical Machines (ICEM)*, 2022, pp. 421-426, doi: 10.1109/ICEM51905.2022.9910702.
- [6] Flankl, Michael et al. "Energy Harvesting With Single-Sided Linear Induction Machines Featuring Secondary Conductive Coating." *IEEE Transactions on Industrial Electronics* 66 (2019): 4880-4890.
- [7] J.K.Nøland, "Prospects and Challenges of the Hyperloop Transportation System: A Systematic Technology Review," in *IEEE Access*, vol. 9, pp. 28439-28458, 2021, doi: 10.1109/ACCESS.2021.3057788.
- [8] Z. Sun, L. Xu, W. Zhao and K. Du, "Comparison Between Linear Induction Motor and Linear Primary Permanent Magnet Vernier Motor for Railway Transportation," *2021 13th International Symposium on Linear Drives for Industry Applications (LDIA)*, Wuhan, China, 2021, pp. 1-6, doi: 10.1109/LDIA49489.2021.9505835.
- [9] Yang Y., Deng J., Tong L., Li X., Peng Q., Zhang W. "Study on the optimization of linear induction motor traction system for fast-speed maglev train" *Transportation Systems and Technology*. - 2018. - Vol. 4. - N. 3 suppl. 1. - P. 156-164. doi: 10.17816/transsyst201843s1156-164
- [10] Bird, J.Z. (2019). "A Review of Integrated Propulsion, Suspension and Guidance Passive Guideway Maglev Technologies." 1-6. 10.1109/LDIA.2019.8770983.
- [11] Abdollahi, Seyed Ehsan et al. "Design and Analysis of a Double-Sided Linear Induction Motor for Transportation." *IEEE Transactions on Magnetics* 51 (2015): 1-7.
- [12] R. C. Creppe, J. A. C. Ulson and J. F. Rodrigues, "Influence of Design Parameters on Linear Induction Motor End Effect," in *IEEE Transactions on Energy Conversion*, vol. 23, no. 2, pp. 358-362, June 2008, doi: 10.1109/TEC.2008.918594.
- [13] H. -T. Cho, Y. -C. Liu and K. A. Kim, "Short-Primary Linear Induction Motor Modeling with End Effects for Electric Transportation Systems," *2018 International Symposium on Computer, Consumer and Control (IS3C)*, Taichung, Taiwan, 2018, pp. 338-341, doi: 10.1109/IS3C.2018.00092.
- [14] S. G. Lee, H. -W. Lee, S. -H. Ham, C. -S. Jin, H. -J. Park and J. Lee, "Influence of the Construction of Secondary Reaction Plate on the Transverse Edge Effect in Linear Induction Motor," in *IEEE Transactions on Magnetics*, vol. 45, no. 6, pp. 2815-2818, June 2009, doi: 10.1109/TMAG.2009.2018669.
- [15] W. -Y. Ji, G. Jeong, C. -B. Park, I. -H. Jo and H. -W. Lee, "A Study of Non-Symmetric Double-Sided Linear Induction Motor for Hyperloop All-In-One System (Propulsion, Levitation, and Guidance)," in *IEEE Transactions on Magnetics*, vol. 54, no. 11, pp. 1-4, Nov. 2018, Art no. 8207304, doi: 10.1109/TMAG.2018.2848292.
- [16] R. Raj, C.Henriksson, P. Subramaniyan & M. Nybacka, "Performance Mapping of a Linear Induction Machine for Hyperloop Applications" in *ICEM 2022*, doi: 10.1109/ICEM51905.2022.9910852
- [17] R. Pedersen, "Design of the Near-Sonic Double-Sided Linear Induction Motor for the Hyperloop Propulsion System", Master Thesis June 2021 at NTNU Trondheim, Accessed 24.08.2022
- [18] Junfei Han, Yaohua Li, Yumei Du, Wei Xu and Nengqiang Jin, "Dynamic characteristics study of single-sided linear induction motor with finite element method," *2008 IEEE/ASME International Conference on Advanced Intelligent Mechatronics*, Xi'an, China, 2008, pp. 439-444, doi: 10.1109/AIM.2008.4601701.
- [19] Linear motion tips, "How do linear induction motors work?", www.linearmotiontips.com/faq-linear-induction-motors-work.
- [20] S. A. Nasar and L. Del Cid, "Propulsion and levitation forces in a single-sided linear induction motor for high-speed ground transportation," in *Proceedings of the IEEE*, vol. 61, no. 5, pp. 638-644, May 1973, doi: 10.1109/PROC.1973.9121.
- [21] F. Gieras, Ph.D., D.Sc., "Simplified theory of double-sided linear induction motor with squirrel-cage elastic secondary" *IEE PROCEEDINGS*, Vol. 130, Pt. B, No. 6, NOVEMBER 1983.
- [22] L. Petrescu, V. Ionita, E. Cazacu & C. Petrescu, "Steinmetz' Parameters Fitting Procedure for the Power Losses Estimation in Soft Magnetic Materials" in *OPTIM 2017 International Conference*, 2017, doi: 10.1109/OPTIM.2017.7974972
- [23] Wikipedia, "Eddy current", [https://en.wikipedia.org/wiki/Eddy\\_current](https://en.wikipedia.org/wiki/Eddy_current)
- [24] Electrical Volt, "Torque-slip Characteristics of Induction Motor", <https://www.electricalvolt.com/2018/12/torque-slip-characteristics-of-induction-motor/>
- [25] Kothari, D.P. and Nagrath, I.J. (2018) "Electric machines. 5th edn." Chennai: McGraw Hill Education (India).
- [26] M. S. Sanjari Nia, M. Altimania, P. Shamsi and M. Ferdowsi, "Electric Field and Parasitic Capacitance Analysis for HF Transformers with Coaxial Winding Arrangements," *2020 IEEE Kansas Power and Energy Conference (KPEC)*, Manhattan, KS, USA, 2020, pp. 1-5, doi: 10.1109/KPEC47870.2020.9167586.

## APPENDIX A COMSOL

### A. Parameters

The following figures are screenshots of the parameters implemented in COMSOL. Parameters for geometry were in a separate parameter designation.

Name	Expression	Value	Description
amplitude	$120 \cdot \sqrt{2}$	169.71	
ang_el_init	0[rad]	0 rad	
f	350[Hz]	350 Hz	Source frequency(base v...
I	70[A]	70 A	Current
J	$8[A/mm^2]$	$8E6 A/m^2$	Current density
k_cu	0.5	0.5	Copper factor
Ns	24	24	Number of statot slots sl...
Ns_teeth	Ns+1	25	Number of stator teeth te...
t	0[s]	0 s	
T	$2 \cdot 1/f$	0.0057143 s	
turns	10	10	
v_s	$2 \cdot t \cdot p \cdot f$	38.675 m/s	
v_x	31[m/s]	31 m/s	

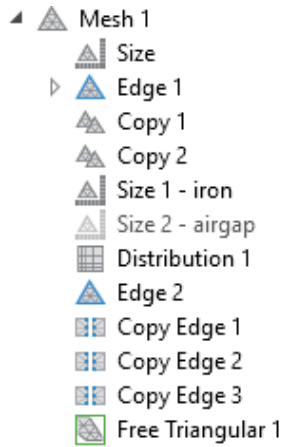
Name	Expression	Value	Description
length_lim	Ns*length_slot...	0.442 m	
thickness_...	20 [mm]	0.02 m	
length_rail	2[m]	2 m	
thickness_...	4 [mm]	0.004 m	
margin	10[mm]	0.01 m	Chosen arbitrarily
height_air	thickness_rail+2...	0.058 m	Air domain height
air_gap	2 [mm]	0.002 m	
length_slot	8 [mm]	0.008 m	
length_to...	10 [mm]	0.01 m	
height_slot	15 [mm]	0.015 m	
height_to...	height_slot	0.015 m	
poles	8	8	
t_p	length_lim/poles	0.05525 m	pole pitch
depth_lim	0.1[m]	0.1 m	
L_p	$2 \cdot t_p + poles \cdot len...$	0.3425 m	length of coil for pole pit...
A_slot	height_slot*len...	$1.2E-4 m^2$	Slot area
A_slot_cu	A_slot*k_cu	$6E-5 m^2$	
N	abs(A_slot_cu/a...	9.6975	Number of turns calculat...
a_cu	$I/(J \cdot \sqrt{2})$	$6.1872E-6 m^2$	Coil wire corss-section ar...
A_wire	a_cu/turns	$6.1872E-7 m^2$	

### B. Geometry and physics

The following figures are screenshots of the Definitions used, geometry built, materials used, physics applied, and mesh created.

- ☰ Definitions
  - 📄 Variables 1
  - 📁 Selections
    - 🔍 Domain Probe 1 (*dom1*)
    - 📐 Integration of I-beam (*int\_a1*)
    - 📐 Integration 2 (*intop2*)
    - 🔗 Identity Boundary Pair 3a (*ap3*)
    - 🔗 Boundary System 1 (*sys1*)
  - 📄 View 1

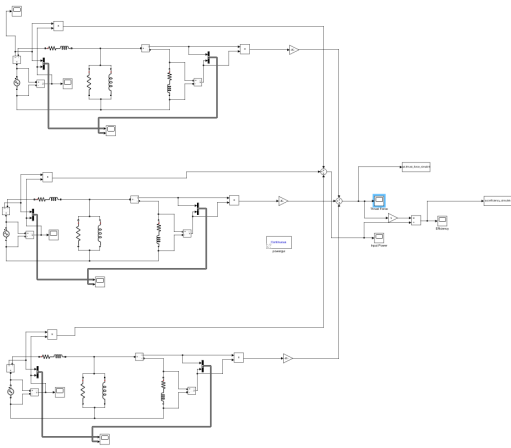
- 📁 Geometry 1
  - 📄 Rail (*r1*)
  - 📄 Air gap (*r5*)
  - 📄 Air gap 2 (*r7*)
  - 📄 LIM yoke (*r3*)
  - 📄 Tooth (*r2*)
  - 📄 Slot (*r4*)
  - 📄 Teeth (*arr1*)
  - 📄 Slots (*arr2*)
  - 📄 LIM Core Selection (*unisel1*)
  - 📄 LIM Core Union (*uni1*)
  - 📄 Air LIM (*r6*)
  - 📄 Air gap 2 + Air LIM (*uni5*)
  - 📄 LIM One side selection (*unisel2*)
  - 📄 LIM One side (*uni2*)
  - 🔗 Air gap mirror (*mir2*)
  - 🔗 LIM Other Side Mirror (*mir1*)
  - 📄 DSLIM Primary Selection (*unisel3*)
  - 📄 DSLIM Primary (*uni3*)
  - 📄 DSLIM Secondary selection (*unisel4*)
  - 📄 DSLIM Secondary (*uni4*)
  - 📄 Form Assembly (*fin*)
- 📁 Materials
  - 📄 Air (*mat2*)
  - 📄 Aluminum 6063-T83 (*mat3*)
  - 📄 Copper (*mat4*)
  - 📄 Soft Iron (Without Losses) (*mat5*)
  - 📄 Silicon Steel NGO 35PN300 (*mat6*)
- 📁 Moving Mesh
  - 🔗 Prescribed Deformation 1
- 📁 Magnetic Fields (*mf*)
  - 📄 Air/Aluminum rail
  - 📄 Magnetic Insulation 1
  - 📄 Initial Values 1
  - 📄 Continuity
  - 🔗 Periodic Condition 1
  - 📄 Iron
  - 📄 Force Calculation 1
  - 📄 Velocity (Lorentz Term) 1
- 📁 Coils
  - 📄 PhaseA
  - 📄 PhaseB
  - 📄 PhaseC



Notes regarding the physics: The "Velocity Lorentz term" is set on the aluminum beam for stationary analysis, and is deactivated for time-dependent analysis. When performing frequency sweeps, the Iron core is set to "Effective BH-Curve", whilst time-dependent simulations use "BH-Curve".

## APPENDIX B SIMULINK/MATLAB

### A. Complete Simulink domain



### B. Raw data and calculations from stationary simulations

DC-test:  $R_1 = 0.0431 \Omega$

No load test: see Table III.

Locked rotor test: see Table IV.

Calculations for Simulink: see Table V.

Operating point voltages: see Table VI.

### C. Scripts to do Simulink simulations and plot results.

#### 1) Simulink simulation script:

```
clear
t_p = 55.25e-03; % The only fixed
→ parameter
% The rest of the parameters change with
→ operating point
f = 200;
v_s = 2*f*t_p;
v = 16.25;
s = 1 - v/v_s;
```

```
R_1 = 0.0431;
R_2 = 0.1931;
L_1 = 1.04e-04;
L_2 = L_1;
R_C = 1.72;
L_m = 5.71e-04;
V_ph = 42.40;
angle = 51.36;
```

#### 2) Plotting force-speed and efficiency characteristics:

```
forcespeedchar =
→ readmatrix("forcespeedcharacteristic.csv");
hold on
plot(forcespeedchar(1:21, 1),
→ forcespeedchar(1:21, 3)); % change
→ columns for efficiency
plot(forcespeedchar(22:61, 1),
→ forcespeedchar(22:61, 3));
plot(forcespeedchar(62:121, 1),
→ forcespeedchar(62:121, 3));
plot(forcespeedchar(122:201, 1),
→ forcespeedchar(122:201, 3));
plot(forcespeedchar(202:302, 1),
→ forcespeedchar(202:302, 3));
plot(forcespeedchar(303:424, 1),
→ forcespeedchar(303:424, 3));
plot(forcespeedchar(425:566, 1),
→ forcespeedchar(425:566, 3));
legend('f = 50 Hz', 'f = 100 Hz', 'f = 150
→ Hz', 'f = 200 Hz', 'f = 250 Hz', 'f =
→ 300 Hz', 'f = 350 Hz')
xlabel('v [m/s]')
ylabel('F [N]')
hold off
```

#### 3) Plotting thrust force results:

```
thrustforce_simu =
→ out.thrust_force_simulink;
thrustforce_stationary = 80.626; %Changes
→ with every simulation point
thrustforce_transient =
→ readmatrix("thrustforce_200Hz.csv");
thrustforce_simu.Name = 'Thrust Force';
hold on
plot(thrustforce_simu)
yline(thrustforce_stationary)
plot(thrustforce_transient(:,1),thrustforce_transient(:,2))
legend('Analytical', 'Stationary',
→ 'Transient')
xlabel('t [s]')
ylabel('F [N]')
hold off
```

#### 4) Plotting efficiency results:

```
efficiency_simu = out.efficiency_simulink;
efficiency_stationary = 0.4527; %Changes
→ with every simulation point
```

**TABLE III:** Parameters from no load test( $F = 0$  N) in stationary simulations in COMSOL.

Frequency[Hz]	No load speed[m/s]	Measured resistance[ $\Omega$ ]	Measured inductance[H]
50	4.978	0.0852	7.91e-04
100	9.769	0.16644	7.02e-04
150	14.728	0.24061	6.36e-04
200	19.823	0.29825	5.91e-04
250	24.946	0.34554	5.57e-04
300	30.104	0.38289	5.29e-04
350	35.27	0.41343	5.06e-04

**TABLE IV:** Parameters from locked rotor test( $v = 0$  m/s) in stationary simulations in COMSOL.

Frequency[Hz]	Measured resistance[ $\Omega$ ]	Measured inductance[H]
50	0.13832	3.75e-04
100	0.16689	2.53e-04
150	0.17623	2.20e-04
200	0.1814	2.08e-04
250	0.18544	2.01e-04
300	0.18906	1.97e-04
350	0.19252	1.95e-04

**TABLE V:** Calculated parameters for the equivalent circuit based on the values from Table III and Table IV.

Frequency[Hz]	$R_1$ [ $\Omega$ ]	$R'_2$ [ $\Omega$ ]	$L_1$ [H]	$L'_2$ [H]	$R_{Fe}$ [ $\Omega$ ]	$L_m$ [H]
50	0.0431	0.1603	1.88e-04	1.88e-04	0.89	6.30e-04
100	0.0431	0.1773	1.26e-04	1.26e-04	1.19	6.43e-04
150	0.0431	0.1857	1.10e-04	1.10e-04	1.44	6.09e-04
200	0.0431	0.1931	1.04e-04	1.04e-04	1.72	5.71e-04
250	0.0431	0.2007	1.01e-04	1.01e-04	2	5.37e-04
300	0.0431	0.2085	9.87e-05	9.87e-05	2.28	5.06e-04
350	0.0431	0.2167	9.74e-05	9.74e-05	2.55	4.77e-04

**TABLE VI:** Voltages for the operating points selected along with stationary results.

Frequency[Hz]	Speed[ $\Omega$ ]	Terminal voltage[V]	Thrust force[N]	Efficiency
50	3	16.57 $\angle$ 53 $^\circ$	98.913	0.27935
100	7.25	27.08 $\angle$ 51.86 $^\circ$	88.88	0.3561
150	11.5	34.71 $\angle$ 50.68 $^\circ$	84.864	0.40752
200	16.25	42.40 $\angle$ 51.36 $^\circ$	80.626	0.4527
250	21.25	50.28 $\angle$ 52.54 $^\circ$	77.575	0.49169
300	26.25	57.75 $\angle$ 53.6 $^\circ$	75.137	0.5239
350	31	63.73 $\angle$ 54.1 $^\circ$	72.807	0.54939

```

efficiency_transient =
    ↪ readmatrix("efficiency_200Hz.csv");
efficiency_simu.Name = 'Efficiency';
hold on
plot(efficiency_simu)
yline(efficiency_stationary)
plot(efficiency_transient(:,1),efficiency_transient(:,2))
legend('Analytical', 'Stationary',
    ↪ 'Transient')
xlabel('t [s]')
ylabel('\eta')
hold off

frequency_list = [50, 100, 150, 200, 250,
    ↪ 300, 350];
efficiency_simu_list = [0.2573, 0.3661,
    ↪ 0.4132, 0.4493, 0.4757, 0.4914,
    ↪ 0.4872]; %end point of simulation
efficiency_stationary_list = [0.27935,
    ↪ 0.40752, 0.4527, 0.49169,
    ↪ 0.5239, 0.54939];
efficiency_transient_high = [0.33081,
    ↪ 0.37811, 0.46717, 0.4901, 0.48066,
    ↪ 0.46667, 0.43553]; %maximum point of
    ↪ last electrical period

```

5) Plotting the collected graph:

```

efficiency_transient_low = [0.27214,
    → 0.24498, 0.17556, 0.12777, 0.12971,
    → -0.043507, -0.23548]; %minimum point
    → of last electrical period
thrustforce_simu_list = [92.5975,
    → 104.9812, 100.7395, 94.7545, 89.7680,
    → 85.4465, 85.4087]; % end point of
    → simulation
thrustforce_stationary_list = [98.913,
    → 88.88, 84.864, 80.626, 77.575, 75.137,
    → 72.807];
thrustforce_transient_high = [118.55,
    → 89.391, 97.621, 82.206, 72.612,
    → 62.999, 53.32]; %maximum point of last
    → electrical period
thrustforce_transient_low = [90.393,
    → 58.045, 35.78, 21.554, 19.361,
    → -5.9607, -29.811]; %minimum point of
    → last electrical period
figure(1);
hold on
plot(frequency_list,
    → efficiency_transient_high, '-');
plot(frequency_list,
    → efficiency_transient_low, '-')
patch([frequency_list
    → fliplr(frequency_list)],
    → [efficiency_transient_low
    → fliplr(efficiency_transient_high)],
    → [0.76 1 0.76]);
plot(frequency_list, efficiency_simu_list,
    → 'x', 'Color', 'b');
plot(frequency_list,
    → efficiency_stationary_list, '.',
    → 'Color', 'r');
legend('', '', 'Transient',
    → 'Analytical', 'Stationary');
xlabel('Frequency [Hz]');
ylabel('\eta');
hold off
figure(2);
hold on
plot(frequency_list,
    → thrustforce_transient_high, '-');
plot(frequency_list,
    → thrustforce_transient_low, '-')
patch([frequency_list
    → fliplr(frequency_list)],
    → [thrustforce_transient_low
    → fliplr(thrustforce_transient_high)],
    → [0.76 1 0.76]);
plot(frequency_list,
    → thrustforce_simu_list, 'x', 'Color',
    → 'b');
plot(frequency_list,
    → thrustforce_stationary_list, '.',
    → 'Color', 'r');
legend('', '', 'Transient',
    → 'Analytical', 'Stationary');
xlabel('Frequency [Hz]');
ylabel('Thrust Force [N]');
hold off
speed_vec = [3, 6.25, 11.5, 16.25, 21.25,
    → 26.25, 31];
losses_simu_list = zeros(1,7);
losses_stationary_list = zeros(1,7);
losses_transient_high = zeros(1,7);
losses_transient_low = zeros(1,7);
for i = 1:7
    losses_simu_list(i) =
    → (thrustforce_simu_list(i)*speed_vec(i)/efficien
    → -
    → thrustforce_simu_list(i)*speed_vec(i));
    losses_stationary_list(i) =
    → (thrustforce_stationary_list(i)*speed_vec(i)/e
    → -
    → thrustforce_stationary_list(i)*speed_vec(i));
    losses_transient_high(i) =
    → (thrustforce_transient_high(i)*speed_vec(i)/eff
    → -
    → thrustforce_transient_high(i)*speed_vec(i));
    losses_transient_low(i) =
    → (thrustforce_transient_low(i)*speed_vec(i)/eff
    → -
    → thrustforce_transient_low(i)*speed_vec(i));
end
copper_losses = 70^2*0.0431*ones(1,7);
hold on
plot(frequency_list,
    → losses_transient_high/1000, '-');
plot(frequency_list,
    → losses_transient_low/1000, '-')
patch([frequency_list
    → fliplr(frequency_list)],
    → [losses_transient_low/1000
    → fliplr(losses_transient_high/1000)],
    → [0.76 1 0.76]);
plot(frequency_list,
    → losses_simu_list/1000, 'x', 'Color',
    → 'b');
plot(frequency_list,
    → losses_stationary_list/1000, '.',
    → 'Color', 'r');
area(frequency_list, copper_losses/1000,
    → 'FaceColor', [0.9294 0.6941 0.1255]);
legend('', '', 'Transient',
    → 'Analytical', 'Stationary', 'Copper
    → losses');

```



```

xlabel('Frequency [Hz]');
ylabel('P_{total}[kW]');
hold off

```

APPENDIX C  
ADDITIONAL RESULTS

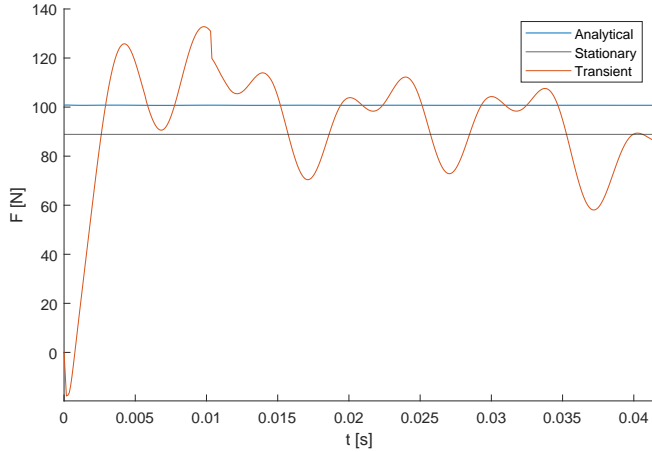


**FIGURE 31:** Thrust force on the aluminum beam for  $f = 100$  Hz and  $v = 7.25$  m/s. The transient results are from the 2D LIM model simulated in a time-dependent moving-mesh study over 4 electrical periods. The sudden drop for transient results around  $t = 0.012$  s was a computational error.

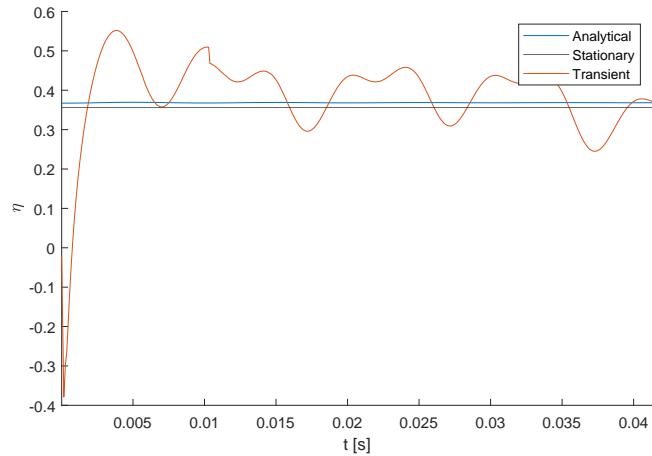


**FIGURE 32:** Efficiency of the LIM for  $f = 100$  Hz and  $v = 7.25$  m/s. The transient results are from the 2D LIM model simulated in a time-dependent moving-mesh study over 4 electrical periods. The sudden drop for transient results around  $t = 0.012$  s was a computational error.

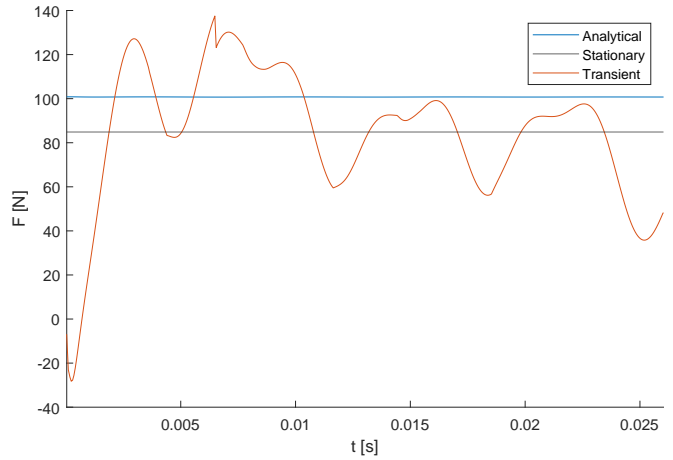


**FIGURE 33:** Thrust force on the aluminum beam for  $f = 150$  Hz and  $v = 11.5$  m/s. The transient results are from the 2D LIM model simulated in a time-dependent moving-mesh study over 4 electrical periods. The sudden drop for transient results around  $t = 0.007$  s was a computational error.

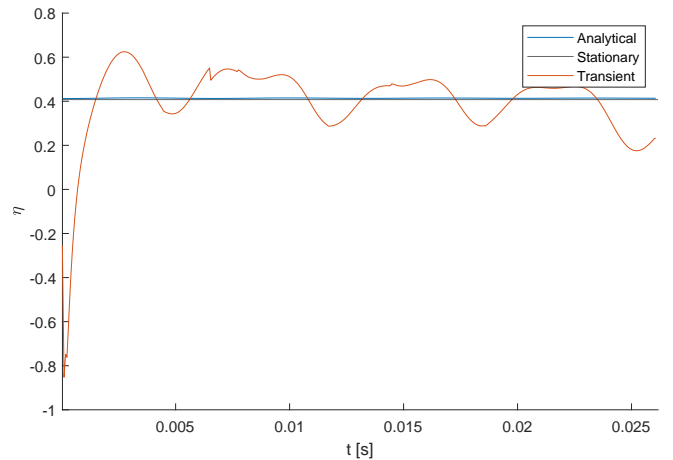


**FIGURE 34:** Efficiency of the LIM for  $f = 150$  Hz and  $v = 11.5$  m/s. The transient results are from the 2D LIM model simulated in a time-dependent moving-mesh study over 4 electrical periods. The sudden drop for transient results around  $t = 0.007$  s was a computational error.

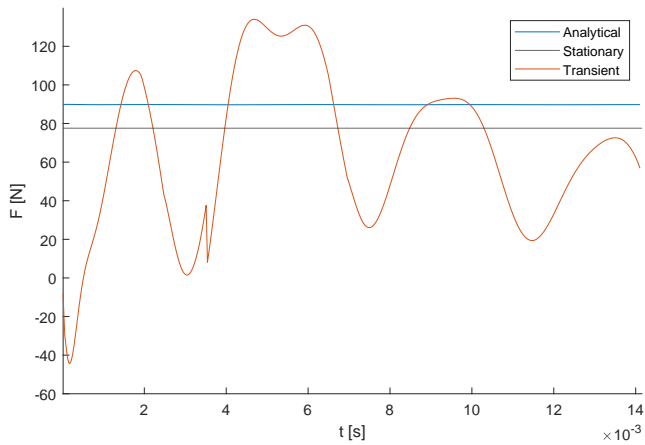


**FIGURE 35:** Thrust force on the aluminum beam for  $f = 250$  Hz and  $v = 21.25$  m/s. The transient results are from the 2D LIM model simulated in a time-dependent moving-mesh study over 4 electrical periods. The sudden drop for transient results around  $t = 0.0035$  s was a computational error.

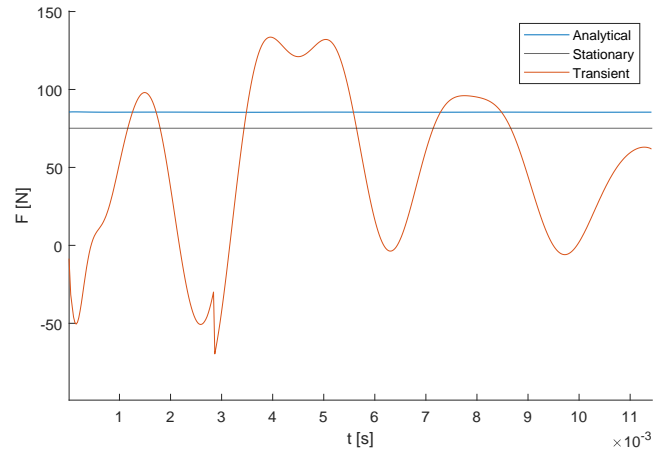


**FIGURE 37:** Thrust force on the aluminum beam for  $f = 150$  Hz and  $v = 26.25$  m/s. The transient results are from the 2D LIM model simulated in a time-dependent moving-mesh study over 4 electrical periods. The sudden drop for transient results around  $t = 0.007$  s was a computational error.

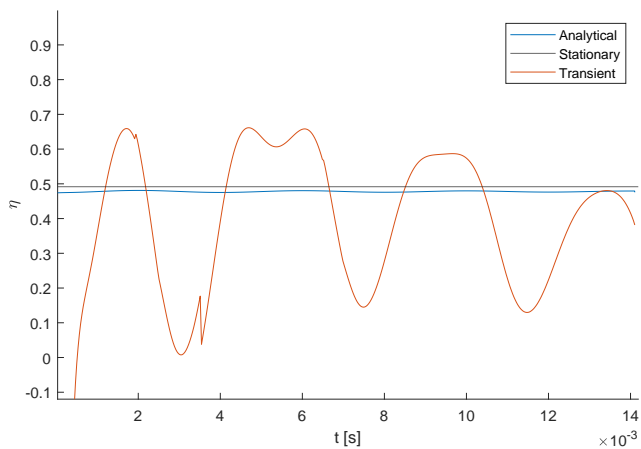


**FIGURE 36:** Efficiency of the LIM for  $f = 250$  Hz and  $v = 21.25$  m/s. The transient results are from the 2D LIM model simulated in a time-dependent moving-mesh study over 4 electrical periods. The sudden drop for transient results around  $t = 0.0035$  s was a computational error.

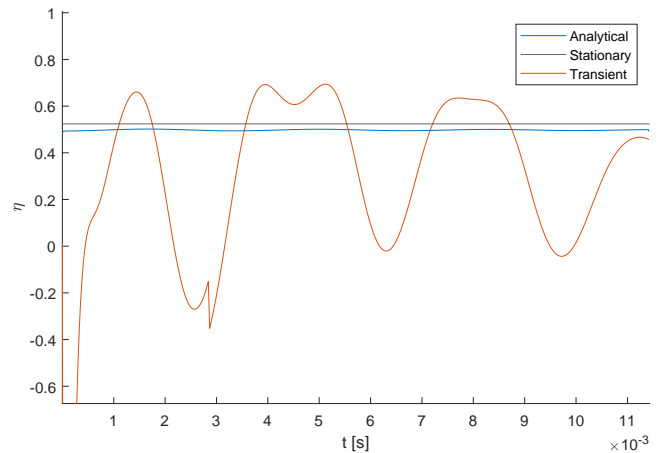


**FIGURE 38:** Efficiency of the LIM for  $f = 150$  Hz and  $v = 26.25$  m/s. The transient results are from the 2D LIM model simulated in a time-dependent moving-mesh study over 4 electrical periods. The sudden drop for transient results around  $t = 0.007$  s was a computational error.



 **NTNU**

Norwegian University of  
Science and Technology